JOURNAL OF MAGNETISM AND MAGNETIC MATERIALS

Editor-in-Chief: Dr. M. Knobel, Inst. de Fisica 'Gleb Wataghin, Universidade Estadual de Campinas (UNICAMP), Rua Sérgio Buarque de Holanda 777, 13.083-859 SP, Campinas, Brazil.

ISSN: 0304-8853; Impact factor = 3.046 (Elsevier)

Accepted May 6th 2019

"MAGNETIC MICRO-SWIMMERS PROPELLING THROUGH BIO-RHEOLOGICAL LIQUID BOUNDED WITHIN AN ACTIVE CHANNEL"

Z. Asghar [a,*], N. Ali[a], M. Sajid[a] *and* **O. Anwar Bég[b]**

[a] *Department of Mathematics and Statistics, IIU, Islamabad 44000,* ***Pakistan***

[b] *Fluid Mechanics and Bio-Propulsion, Aeronautical and Mechanical Engineering Department, School of Computing, Science and Engineering (CSE), G77, Newton Building, University of Salford, M54WT,* ***UK***

ABSTRACT:

The dynamics of a micro-organism swimming through a channel with undulating walls subject to constant transverse applied magnetic field is investigated. The micro-organism is modeled as self-propelling undulating sheet which is out of phase with the channel waves while the electrically-conducting biofluid (through which micro-swimmers propel) is characterized by the non-Newtonian shear-rate dependent Carreau fluid model. Creeping flow is mobilized in the channel due to the self-propulsion of the micro-organism and the undulatory motion of narrow gapped walls. Under these conditions the conservation equations are formulated under the long wavelength and low Reynolds number assumptions. The speed of the self-propelling sheet and the rate of work done at higher values of rheological parameters are obtained by using a hybrid numerical technique (MATLAB routine bvp-4c combined with a modified Newton-Raphson method). The results are validated through an alternative hybrid numerical scheme (implicit finite difference method (FDM) in conjunction with a modified Newton-Raphson method). The assisting role of magnetic field and rheological effects of the surrounding biofluid on the swimming mode are shown graphically and interpreted at length. The global behavior of biofluid is also expounded via visualization of the streamlines in both regions (above and below the swimming sheet) for realistic micro-organism speeds. The computations reveal that optimal swimming conditions for the micro-organism (i.e., greater speed with lower energy losses) are achievable in magnetohydrodynamic (MHD) environments including magnetic field-assisted cervical treatments.

Keywords: *Micro-organism; peristaltic (active) channel; Carreau fluid; Swimming speed; bio-magnetohydrodynamics (bioMHD); Rate of work done; Hybrid numerical method, Newton-Raphson method; Cervical magnetic therapy.*

**Corresponding author. Tel.: + 923455882685; E-mail address: zee.qau5@gmail.com*

1. INTRODUCTION

Mathematical models describing the dynamics of swimming microorganisms such as spermatozoa have attracted the attention of researchers for many decades. In this context, **Taylor [1]** communicated the original analysis concerning the hydrodynamics of spermatozoa by approximating the micro-organism surface as an infinite sinusoidal sheet in an unbounded Newtonian liquid. He deployed the lubrication approximation and a perturbation approach to compute the swimming speed and power dissipation. Following the same methodology **Taylor [2]** extended his previous work by replacing the infinite oscillating *sheet* with an infinite oscillating *cylindrical filament*. Inspired by the pioneering work of **Taylor [2]**, **Hancock [3]** calculated the propelling speed of undulating cylindrical filament by employing the Stokeslet distribution technique. In another article, the speed of sea urchin spermatozoa was computed successfully by **Gray and Hancock [4].** Taylor's problem was further extended by **Drummond [5]** for larger wave amplitudes. **Reynolds [6]** and **Tuck [7]** included inertial effects in Taylor's model by introducing Reynolds number in the analysis. The above articles addressed analytically the swimming problem in an *unbounded domain*. However actual micro-organisms in internal physiology (e.g. spermatozoa) swim through narrow passages to reach their destination. This important characteristic was first appraised theoretically by **Reynolds [6]** to analyse swimming of a wavy sheet near to a rigid plane wall, identifying that in the vicinity of the solid boundaries swimming motion tends to create a distinct *shear pattern* which leads the spermatozoa away from the wall. Later, **Shack and Lardner [8]** and **Katz [9]** utilized lubrication theory to examine the wavy sheet hydrodynamics swimming between two rigid walls. **Shukla *et al.* [10]** explored the swimming propulsion of sperm bounded within rigid channel with peripheral layer viscosity and dynamical interactions. Sperm intrinsic movements do not appear to be the only force directing them toward the oviducts. In fact, such motions are superimposed with the peristaltic motion of the walls of the uterus and cervix. Thus, the muscular contractions of the cervical canal can also play an important role in influencing the sperm motility. Keeping this fact in mind, **Smelser *et al*. [11]** established a biofluid mechanical model for the sperm transport in a peristaltic cervical channel. **Shukla *et al.* [12]** theoretically analysed the motion of micro-swimmers through oscillating walls using the long wavelength approximation. The significant effects of variable viscosity on the swimming mechanism (*via simulation of a self-propelling sheet in a channel with*

and without peristalsis) was later quantified by **Radhakrishnamacharya and Sharma [13].** Further, a recent study by **Walait *et al*. [14]** constitutes a significant contribution to the existing literature in this regard. The theoretical analysis described in **[14]** deals with the hydrodynamics of a swimming sheet *with heat transfer* through non-isothermal Newtonian cervical liquid in a deformable channel comprising two oscillating walls inclined at a certain angle.

Sperm motility also refers to how well the sperm in a given semen sample/cervical mucus are moving. It is therefore essential to analyze sperm-fluid interaction with assisting rheological conditions by treating cervical fluid as *non-Newtonian* since actual cervical fluid exhibits significant rheological characteristics which deviate from the classical Newtonian model. Several robust efforts have been made in this regard and may be viewed as *extensions* of Taylor's swimming sheet problem in an unbounded liquid and the problems attempted by **Reynolds [6]** and **Semelsar *et al.* [11]**. The first formal attempt to extend the Taylor's swimming sheet problem in an unbounded liquid characterized by a viscoelastic second order (differential Reiner-Rivlin) fluid was made by **Chaudhry [15]. Sturges [16]** further extended **Chaudhry's** work with a more complex integral constitutive equation representing the fluid around the organism. Extending Taylor's model for MHD second order fluid **Sajid *et al.* [17]** clarified and corrected an erroneous computation in Chaudhry's work. The role of a variety of non-Newtonian models in improving the swimming efficiency i.e. faster propulsion with less energy losses in an unbounded domain, was elaborated in excellent detail by **Lauga [18]. Sajid *et al.* [19]** incorporated the feature of porous medium drag in the Lauga model. **Ali *et al.* [20]** considered couple stress effects in an unbounded fluid as the propulsion medium for the swimmer. An even more sophisticated microstructural rheological approach, utilizing the celebrated *Eringen micropolar* model, was expounded by **Sinha *et al.* [21]** and **Phillip and Chandra [22]** to investigate hydrodynamic propulsion in microstructural rheological media. The rigid boundary was examined by **Balmforth et al [23]** for swimming in simple viscoplastic (Bingham) fluids. **Ives and Morozov [24]** attempted a parallel problem for the more elegant viscoelastic Oldroyd-B fluid wherein an important parametric study of organism speed and flow fields generated by the swimmer were calculated with a spectral numerical method. In the present article, we present a detailed analysis to explore the dynamics of infinite wavy sheet in an active/passive channel filled with magnetic (electrically-conducting) non-Newtonian Carreau biofluid. The model problem corresponds to the

movement of spermatozoa through the cervical canal under an externally imposed magnetic field and aims to simulate *specific cervical magnetic therapy techniques*. Magnetic therapy involves the deployment of a specific magnet with a sticky substance close to the human body. It has been identified via clinical investigations that this methodology increases circulation, so it can be used as an external treatment for any sort of injury to the tissues. Since human health is immensely dependent on the efficient movement of biofluids (especially blood) via for example the cardiovascular, embryological and other physiological systems, it is crucial to mitigate the stagnation of physiological fluids very quickly. Via magnetic therapy (increasing circulation) clinical engineers can robustly increase the tissue nutrition and can also remove waste products and maintain efficient, unobstructed flows. Ensuring sustained and successful continuous transport of biofluids in the human body therefore greatly assists and benefits health. Magnetic neck support, magnetic bracelets, magnetic shoes and magnetic beds constitute some different mechanisms of bio-magnetic assistance to the human body via extra-corporeal magnetic fields. A further advantage of magnetic therapy is that it does not have side-effects and is non-intrusive and therefore an excellent alternative to conventional surgical methods which may be traumatic.

The non-Newtonian Carreau model involves four rheological parameters: *power law index, relaxation time, and both low and high shear rates viscosity constants* and is found to be superior to other generalized Newtonian fluid models in predicting the rheology of many actual physiological (embryological) fluids **[25].** More recently this model has been utilized by **Cordero and Lauga [26]** to generalize Taylor's swimming sheet problem to the *non-Newtonian* case. However, this model has not been utilized to explore the dynamics of a swimming micro-organism (infinite wavy sheet) in an active/passive channel with magnetohydrodynamics. This topic is greatly relevant to bio-magnetic therapy and magnetic-assisted embryological clinical methods which are becoming increasingly popular. Some applications of Carreau and other rheological models including *peristaltic flow* (fluid flow intercalated between two wavy walls), *bacterial gliding* (swimming near a solid wall) and *stagnation point flow* problems in the presence and absence of magnetic field are documented in **refs. [27-37].**

The relevance of magnetohydrodynamic simulation in bio-rheological swimming micro-dynamics (under the imposition of static applied magnetic field) is also motivated by numerous emerging applications including *steering of the swimming of micro-magneto-bots* (deployed in non-invasive gastro-intestinal examinations) **[38]**, magnetofluid dynamic treatment of diseased eyes via targeted

drug delivery **[39]** and sensing/monitoring of the performance of prosthetic smart magneto-rheological kneecaps **[40]**. Further, the green magneto-tactic microbial fuel cells for energy generation also utilize magnetic swimming **[41, 42]**. The works of **Ansari *et al.* [43, 44]** on the swimming of micro-organisms in a hydromagnetic fluid, **Gadelha [45]** on swimming under the effects of oscillating magnetic field, **Belovs and Cebers [46]** on ferromagnetic micro-swimmers, **Goa *et al.* [47]** on fuel-free magnetic swimming for targeted drug delivery and **Gauger *et al.* [48]** on artificial magnetic cilia motion at low Reynolds number also provide a strong motivation for including magnetohydrodynamic effects in swimming sheet spermatozoa propulsion simulations. A recent study by **Asghar *et al.* [53]** dealing with the improvement of swimming efficiency by using Johnson-Segalman rheological fluids is also worthwhile to mention.

The present work which describes the *first analytical and numerical investigation of magnetic micro-swimmer cervical hydrodynamic propulsion in electrically-conducting Carreau embryological biofluids*, is prepared as follows: The schematic diagram and constitutive equations of a *Carreau* model are presented in section **2**. Formulation of the problem under low Reynolds number and long wavelength approximation is described in section **3**. In section **4**, the solution procedure is elaborated in detail along with the exact expressions of propulsive speed and flow rate for the Newtonian case. The numerical method to validate the results obtained is section **4** is described at length in section **5**. In section **6**, the effects of important parameters on swimming speed, energy consumption and streamline plots are shown graphically and discussed in detail. The paper is concluded in section **7** with recommendations also provided for future pathways including electro-fluid rheological micro-organism swimming dynamics.

2. GEOMETRICAL INTERPRETATION AND CERVICAL FLUID EQUATIONS

The geometry of the model describing the two-dimensional swimming of a micro-organism with speed V_s through a cervical channel with wavy walls is illustrated in **Fig. 1** and represents sperm swimming in cervical magnetic therapy.

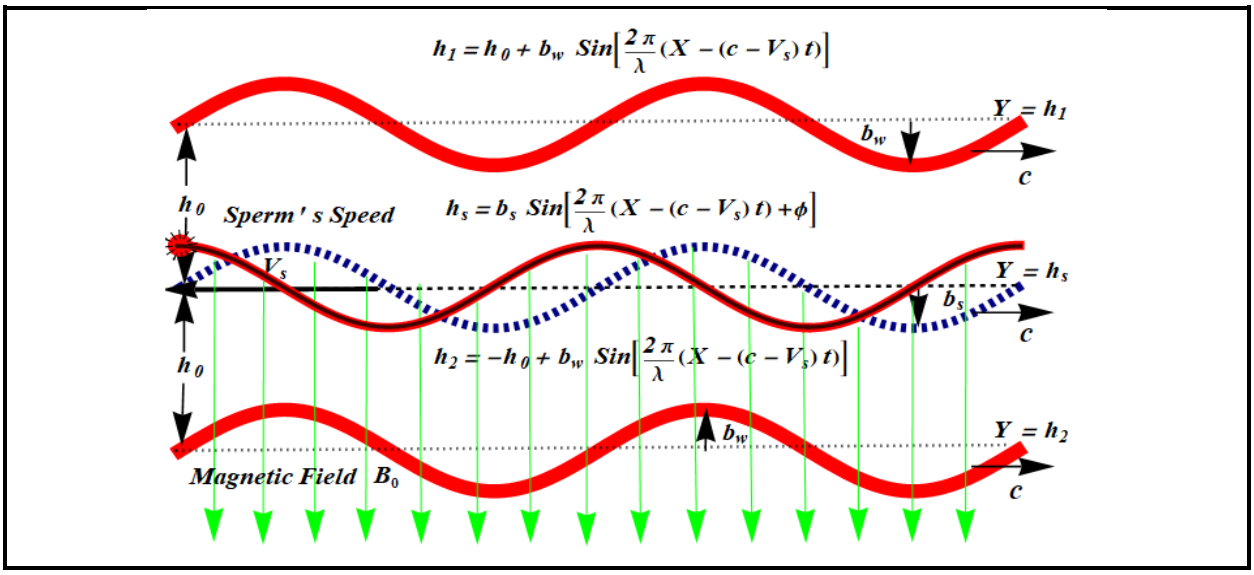

Fig.1. Propulsive motion of a micro-organism in a channel filled with magnetic Carreau fluid.

The fluid inside channel is characterized by an electrically-conducting Carreau fluid model while the micro-swimmer is simulated as an infinite Taylor wavy sheet, propelling in the negative *X*-direction with travelling wave of speed *c* and wavelength λ on its surface. The undulating channel walls and self-propulsion of the spermatozoa generate flow in the positive *X*-direction. A constant magnetic field $\mathbf{B_0} = [0, -B_0, 0]$ of strength B_0 is imposed in opposition of transverse to the swimming direction i.e. in the negative *Y*-direction. The wave profiles h_1 and h_2 propagating along the cervical channel walls and h_s in the organism's tail in the fixed frame are given as **[11-14, 22]**:

$$h_1 = h_0 + b_w \sin\left[\frac{2\pi}{\lambda}\left(X-\left(c-V_s\right)t\right)\right], \qquad \textbf{\textit{(Upper wall)}} \quad (1)$$

$$h_s = b_s \sin\left[\frac{2\pi}{\lambda}\left(X-\left(c-V_s\right)t\right)+\phi\right], \qquad \textbf{\textit{(Surface of the organism)}} \quad (2)$$

$$h_2 = -h_0 + b_w \sin\left[\frac{2\pi}{\lambda}\left(X-\left(c-V_s\right)t\right)\right], \qquad \textbf{\textit{(Lower wall)}} \quad (3)$$

where h_0 denotes the mean distance of the micro-organism swimmer to either of the cervical wall (upper or lower), ϕ is the phase difference with range $0 \le \phi \le \pi$, b_s and b_w are the amplitude of the wave on the micro-organism swimmer surface and cervical walls, respectively. In **Fig. 1** $\phi = 0$ corresponds to the synchronized swimmer (shown by blue dashed line) while $\phi > 0$ corresponds

to the non-synchronized swimmer (shown by red solid line). Since synchrony will not persist practically, therefore it is advisable to consider occasions when the swimmer is *out of phase* with the walls. The organism is fixed with respect to the wave frame which has relative velocity of $c - V_s$.

The appropriate boundary conditions in the fixed frame are given as **[12-15, 23, 53]**:

$$\left.\begin{array}{l} U^{\pm} = 0 \\ V^{\pm} = 0 \end{array}\right\} \begin{array}{l} at\ Y = h_1 \\ \text{and}\, Y = h_2 \end{array}, \quad \textbf{\textit{(Upper and lower channel walls)}} \qquad (4)$$

$$\left.\begin{array}{l} U^{\pm} = -V_s \\ V^{\pm} = -\dfrac{dh_s}{dt} \end{array}\right\} at\ Y = h_s. \quad \textbf{\textit{(Micro-organism swimmer surface)}} \qquad (5)$$

Here $U^{\pm}, V^{\pm}$ are the horizontal and vertical components of velocity field in the laboratory frame. The lower $\left(h_2 \le Y \le h_s\right)$ and upper $\left(h_s \le Y \le h_1\right)$ halves of the channel are denoted respectively by the superscripts (+) and (-). The steady locomotion of the massless wavy organism necessitates that the total force on swimmer surface must be zero **[8-14, 21, 22, 53],** which mathematically takes the form:

$$\int (\mathbf{T}^{+} + \mathbf{T}^{-})\, ds = 0, \qquad (6)$$

Here $\mathbf{T}^{\pm}$ is the force due to the cervical liquid acting on the swimming organism from both sides. The equations that govern incompressible viscous flow of a magnetohydrodynamic (MHD) Carreau fluid (cervical liquid contains ions and other suspensions which respond to an externally applied magnetic field) due to propagating waves on the spermatozoa surface and channel walls, in the low magnetic Reynolds number limit (permitting the omission of induced magnetic field effects) may be written as:

$$\nabla . \mathbf{V}^{\pm} = 0, \quad \textbf{\textit{(Continuity equation)}} \qquad (7)$$

$$\rho \frac{d\mathbf{V}^{\pm}}{dt} - \sigma_m B_o^2 U^{\pm} \mathbf{i} = -\nabla p^{\pm} + \nabla . \boldsymbol{\tau}^{\pm}, \quad \textbf{\textit{(Momentum equation)}} \qquad (8)$$

where ρ is the density of electrically-conducting (magnetic) Carreau cervical fluid, d/dt is the material time derivative, $\mathbf{V}^{\pm}$ is the velocity profile, σ_m is the electrical conductivity of the magnetic Carreau cervical fluid, ***i*** is the unit vector in the *x*-direction, $p^{\pm}$ is the pressure and $\boldsymbol{\tau}^{\pm}$ is the extra stress tensor. The extra stress tensor for the *Carreau* model is **[27-29, 33, 36, 37]**:

$$\boldsymbol{\tau}^{\pm} = 2\left(\mu_{\infty} + (\mu_0 - \mu_{\infty})\left(1 + \Gamma^2 \left(\Pi^{\pm}\right)^2\right)^{\frac{n-1}{2}} \right)\mathbf{D}^{\pm}. \tag{9}$$

Here μ_{∞} is the infinite shear-rate viscosity, μ_0 is the zero shear-rate viscosity, Γ is the time constant and n is the rheological power law index ($n<1$ for shear-thinning fluid, $n=1$ for Newtonian fluid and $n>1$ for shear-thickening fluid). Further, the first Rivlin-Ericksen tensor $\mathbf{D}^{\pm}$ and its magnitude $\Pi^{\pm}$ is defined as:

$$\mathbf{D}^{\pm} = \frac{\left(\nabla \mathbf{V}^{\pm}\right) + \left(\nabla \mathbf{V}^{\pm}\right)^T}{2}, \quad \Pi = \sqrt{2\left(\mathbf{D}^{\pm} : \mathbf{D}^{\pm}\right)} = \sqrt{2trace\left(\left(\mathbf{D}^{\pm}\right)^2\right)}. \tag{10}$$

The fixed and moving (laboratory) frames are related as follows:

$$\begin{aligned} x &= X - (c - V_s)t, \quad y = Y, \\ u^{\pm} &= U^{\pm} - (c - V_s), \quad v^{\pm} = V^{\pm}, \quad P^{\pm} = p^{\pm}, \end{aligned} \tag{11}$$

3. MAGNETOHYDRODYNAMIC NON-NEWTONIAN PROPULSION MODEL

The active cervical walls and propelling microorganism generate a two-dimensional flow with velocity profile $\mathbf{V}^{\pm} = \left[u^{\pm}, v^{\pm}, 0\right]$. **Eqns. (7) and (8)** can be shown to take the following form:

$$\frac{\partial u^{\pm}}{\partial x} + \frac{\partial v^{\pm}}{\partial y} = 0, \tag{12}$$

$$\rho\left(u^{\pm}\frac{\partial}{\partial x} + v^{\pm}\frac{\partial}{\partial y}\right)u^{\pm} - \sigma_m B_0^2 u^{\pm} = -\frac{\partial p^{\pm}}{\partial x} + \frac{\partial \tau^{\pm}{}_{xx}}{\partial x} + \frac{\partial \tau^{\pm}{}_{xy}}{\partial y}, \tag{13}$$

$$\rho\left(u^{\pm}\frac{\partial}{\partial x} + v^{\pm}\frac{\partial}{\partial y}\right)v^{\pm} = -\frac{\partial p^{\pm}}{\partial y} + \frac{\partial \tau^{\pm}{}_{xy}}{\partial x} + \frac{\partial \tau^{\pm}{}_{yy}}{\partial y}, \tag{14}$$

$$\tau^{\pm}{}_{xx} = 2\left(\eta_\infty + (\eta_0 - \eta_\infty)\left(1+\Gamma^2\left(\Pi^{\pm}\right)^2\right)^{\frac{n-1}{2}}\right)\left(\frac{\partial u^{\pm}}{\partial x}\right), \tag{15}$$

$$\tau^{\pm}{}_{xy} = \left(\eta_\infty + (\eta_0 - \eta_\infty)\left(1+\Gamma^2\left(\Pi^{\pm}\right)^2\right)^{\frac{n-1}{2}}\right)\left(\frac{\partial u^{\pm}}{\partial y} + \frac{\partial v^{\pm}}{\partial x}\right), \tag{16}$$

$$\tau^{\pm}{}_{yy} = 2\left(\eta_\infty + (\eta_0 - \eta_\infty)\left(1+\Gamma^2\left(\Pi^{\pm}\right)^2\right)^{\frac{n-1}{2}}\right)\left(\frac{\partial v^{\pm}}{\partial y}\right), \tag{17}$$

where

$$\left(\Pi^{\pm}\right)^2 = \left(\left(\frac{\partial u^{\pm}}{\partial x}\right)^2 + \left(\frac{\partial v^{\pm}}{\partial y}\right)^2\right) + \frac{1}{2}\left(\frac{\partial u^{\pm}}{\partial y} + \frac{\partial v^{\pm}}{\partial x}\right)^2. \tag{18}$$

Introducing the following dimensionless variables and numbers:

$$\begin{gathered} x^* = \frac{2\pi}{\lambda}x,\ y^* = \frac{y}{h_0},\ \left(u^{\pm}\right)^* = \frac{u^{\pm}}{c},\ \ \left(v^{\pm}\right)^* = \frac{v^{\pm}}{\delta c},\ \left(p^{\pm}\right)^* = \frac{2\pi h_0^2}{\lambda\mu_0 c}p^{\pm},\ \left(\tau^{\pm}{}_{ij}\right)^* = \frac{h_0}{\mu_0 c}\tau^{\pm}{}_{ij}, \\ \left(\Pi^{\pm}\right)^{2^*} = \frac{h_0}{c}\left(\Pi^{\pm}\right)^2,\ b_i^* = \frac{b_i}{h_0},\ V_s^* = \frac{V_s}{c},\ Q^* = \frac{Q}{c},\ W^* = \frac{2\pi h_0}{\lambda\mu_0 c^2}W, \\ \delta = \frac{2\pi h_0}{\lambda},\ Re = \frac{\rho c h_0}{\mu_0},\ We = \frac{\Gamma c}{h_0},\ \beta = \frac{\mu_\infty}{\mu_0},\ H^2 = \frac{\sigma_m}{\mu_0 h_0^2}B_0^2, \end{gathered} \tag{19}$$

Next, we define the stream function by the Cauchy-Riemann relations:

$$\left(u^{\pm}\right)^* = \frac{\partial\psi^{\pm}}{\partial y^*},\ \ \left(v^{\pm}\right)^* = -\frac{\partial\psi^{\pm}}{\partial x^*}, \tag{20}$$

It emerges that **Eqn. (12)** is identically satisfied and **Eqns. (13) - (18)** can be written as:

$$\delta Re\left(\left(\frac{\partial\psi^{\pm}}{\partial y}\frac{\partial}{\partial x} - \frac{\partial\psi^{\pm}}{\partial x}\frac{\partial}{\partial y}\right)\left(\frac{\partial\psi^{\pm}}{\partial y}\right)\right) - H^2\frac{\partial\psi^{\pm}}{\partial y} + \frac{\partial p^{\pm}}{\partial x} = \delta\frac{\partial}{\partial x}\tau^{\pm}{}_{xx} + \frac{\partial}{\partial y}\tau^{\pm}{}_{xy}, \tag{21}$$

$$-\delta^3 Re\left[\left(\frac{\partial\psi^{\pm}}{\partial y}\frac{\partial}{\partial x} - \frac{\partial\psi^{\pm}}{\partial x}\frac{\partial}{\partial y}\right)\left(\frac{\partial\psi^{\pm}}{\partial x}\right)\right] + \frac{\partial p^{\pm}}{\partial y} = \delta^2\frac{\partial}{\partial x}\tau^{\pm}{}_{xy} + \delta\frac{\partial}{\partial y}\tau^{\pm}{}_{yy}, \tag{22}$$

$$\tau^{\pm}{}_{xx} = 2\delta\left(\beta+(1-\beta)\left(1+We^2\left(\Pi^{\pm}\right)^2\right)^{\frac{n-1}{2}}\right)\left(\frac{\partial^2\psi^{\pm}}{\partial x\partial y}\right), \tag{23}$$

$$\tau^{\pm}{}_{xy} = \left(\beta+(1-\beta)\left(1+We^2\left(\Pi^{\pm}\right)^2\right)^{\frac{n-1}{2}}\right)\left(\frac{\partial^2\psi^{\pm}}{\partial y^2}-\delta^2\frac{\partial^2\psi^{\pm}}{\partial x^2}\right), \tag{24}$$

$$\tau^{\pm}{}_{yy} = 2\delta\left(\beta+(1-\beta)\left(1+We^2\left(\Pi^{\pm}\right)^2\right)^{\frac{n-1}{2}}\right)\left(\frac{\partial^2\psi^{\pm}}{\partial x\partial y}\right). \tag{25}$$

The dimensionless form of $\Pi^{\pm}$ is given by:

$$\left(\Pi^{\pm}\right)^2 = 2\left(\delta\frac{\partial^2\psi^{\pm}}{\partial x\partial y}\right)^2+\frac{1}{2}\left(\frac{\partial^2\psi^{\pm}}{\partial y^2}-\delta^2\frac{\partial^2\psi^{\pm}}{\partial x^2}\right)^2. \tag{26}$$

In the above equations, the superscript * is omitted for brevity. The parameters $H, We, Re \text{ and } \delta$ denote respectively the *Hartmann (magnetic body force) number*, *Weissenberg number, Reynolds number* (based on channel semi-depth) and *dimensionless wave number*. Now employing the long wavelength and low Reynolds number assumptions, expressions **(23)-(26)** gives $\tau^{\pm}{}_{xx} = 0,$ $\tau^{\pm}{}_{xy} = \left(\beta+(1-\beta)\left(1+We^2\left(\Pi^{\pm}\right)^2\right)^{\frac{n-1}{2}}\right)\left(\frac{\partial^2\psi^{\pm}}{\partial y^2}\right),$ $\tau^{\pm}{}_{yy} = 0$ and $\left(\Pi^{\pm}\right)^2 = \frac{1}{2}\left(\frac{\partial^2\psi^{\pm}}{\partial y^2}\right)^2$. The above assumptions are already popular in mathematical models of micro-organism swimming problems **[1-10, 12-22, 53],** peristaltic flow problems **[27-32]** and bacterial gliding problems **[33-35].** These results when combined with the reduced **Eqn. (21)** lead to:

$$\frac{\partial p^{\pm}}{\partial x} = \frac{\partial}{\partial y}\left\{\left(\beta+(1-\beta)\left(1+We^2\left(\frac{\partial^2\psi^{\pm}}{\partial y^2}\right)^2\right)^{\frac{n-1}{2}}\right)\left(\frac{\partial^2\psi^{\pm}}{\partial y^2}\right)\right\}+H^2\frac{\partial\psi^{\pm}}{\partial y}. \tag{27}$$

Eliminating the *axial pressure gradient* from the reduced **Eqn. (22) and Eq. (27)**, we arrive at:

$$\frac{\partial^2}{\partial y^2}\left\{\left(\beta+(1-\beta)\left(1+We^2\left(\frac{\partial^2\psi^{\pm}}{\partial y^2}\right)^2\right)^{\frac{n-1}{2}}\right)\left(\frac{\partial^2\psi^{\pm}}{\partial y^2}\right)\right\}+H^2\left(\frac{\partial^2\psi^{\pm}}{\partial y^2}\right)=0. \tag{28}$$

Eqn. (28) is subject to following *non-dimensional* boundary conditions:

$$\left.\begin{aligned}\psi^{\pm}=0,\quad \frac{\partial\psi^{\pm}}{\partial y}=V_s-1\\ \frac{\partial\psi^{\pm}}{\partial x}=0\end{aligned}\right\}\ at\ y=h_1=-1+b_w\sin x \\ and\ y=h_2=1+b_w\sin x, \tag{29}$$

$$\left.\begin{aligned}\psi^{\pm}=\mp Q,\quad \frac{\partial\psi^{\pm}}{\partial y}=-1\\ \frac{\partial\psi^{\pm}}{\partial x}=-b_s\cos x\end{aligned}\right\}\ at\ y=h_s=b_s\sin(x+\phi). \tag{30}$$

The volumetric flow rate Q across the channel is computed via integration as:

$$Q=\int_{y=-1+b_w\sin x}^{y=b_s\sin x}\frac{\partial\psi^{-}}{\partial y}dy=\int_{y=b_s\sin x}^{y=1+b_w\sin x}\frac{\partial\psi^{+}}{\partial y}dy. \tag{31}$$

The fluid velocities on either side of the swimmer depend upon b_s, b_w, β, We, n and two unknowns i.e. the propulsive velocity of the sheet V_s and flow rate of the fluid Q. Using the appropriate stress-strain relation with the long wavelength assumption **(see [8-14, 21, 22, 53]),** the *force equilibrium* condition **(7)** gives:

$$\int_{-\pi}^{\pi}\left\{\left[\tau_{xy}\left(V_p,Q;x\right)\right]_{y=bSin(x)}-b_s\,sin(x)\left[\frac{dp\left(V_p,Q;x\right)}{dx}\right]\right\}dx\ = \\ \int_{-\pi}^{\pi}\left\{\left(\tau_{xy}^{+}\left(V_p,Q;x\right)-\tau_{xy}^{-}\left(V_p,Q;x\right)\right)_{y=bSin(x)}-b_s\,sin(x)\left(\frac{dp^{+}\left(V_p,Q;x\right)}{dx}-\frac{dp^{-}\left(V_p,Q;x\right)}{dx}\right)\right\}dx=0. \tag{32}$$

In **Eqn. (32)** the notation [f] indicates the difference in quantity f evaluated above and below the wavy sheet.

In the *free channel* case:

$$\Delta P_\lambda = \int_{-\pi}^{\pi} \frac{dp^{\pm}}{dx} dx = p^{\pm}(\pi) - p^{\pm}(-\pi) = 0. \tag{33}$$

The *rate of work done* (i.e. mechanical energy dissipated) by the micro-organism is given as:

$$W = \int_{-\pi}^{\pi} n_j [\tau_{ji}] u^{\pm}{}_i \, ds \;\; = \int_{-\pi}^{\pi} n_j (\tau_{ji}^{+} - \tau_{ji}^{-}) \frac{\partial \psi^{\pm}{}_i}{\partial y} ds, \tag{34}$$

where n_j and $u^{\pm}{}_i$ designate respectively the unit vector normal to the swimming sheet and velocities of the fluid particle above/below the micro-swimmer in the fixed frame. Also $t^{\pm}_{ji}$ denotes the stress acting on the upper and lower surface of the swimmer. For the long wavelength case, **Eqn. (34)** takes the following form:

$$W(V_p, Q) = \int_{-\pi}^{\pi} b_s \cos x \left[p(V_p, Q; x) \right] dx = \int_{-\pi}^{\pi} b_s \, cos(x) \left(p^{+} - p^{-} \right) dx. \tag{35}$$

4. SOLUTION METHODOLOGY

For the Newtonian case $(We = 0 \; or \; n = 1)$ without MHD effects i.e. electrically non-conducting biofluid case $(H = 0)$, one can find the closed form expressions of $\psi^{\pm}$, $\frac{dp^{\pm}}{dx}$, ΔP_λ as follows:

$$\psi^{\pm} = -\frac{Q(\pm 1 + b_w sinx - y)^2 (\pm 1 + b_w sinx - 3b_s sinx + 2y)}{(\pm 1 + b_w sinx - b_s sinx)^3} + \frac{(\pm 1 + b_w sinx - y)(b_s sinx - y)(\pm 1 + sinx(b_w + b_s - b_s V_s) - 2y + V_s y)}{(\pm 1 + b_w sinx - b_s sinx)^2}, \tag{36}$$

$$\frac{dp^{\pm}}{dx} = \frac{6(-2Q + (\pm 1 + b_w Sinx - b_s Sinx)(-2 + V_s))}{(\pm 1 + b_w Sinx - b_s Sinx)^3}, \tag{37}$$

$$\Delta P_\lambda = -\frac{12\sqrt{-\frac{1}{-1 + (b_s - b_w)^2}}\pi \left(2 + 2Q - V_s + (b_s - b_w)^2 (-2 + Q + V_s)\right)}{\left(-1 + (b_s - b_w)^2\right)^2} = 0, \tag{38}$$

Similarly, the equilibrium condition (32) gives:

$$\frac{12\sqrt{-\frac{1}{-1+\left(b_w-b_s\right)^2}}\pi\left(1+Q+\left(b_w-b_s\right)\left(b_w^{\,3}-b_w^{\,2}b_s+b_s^{\,3}-2b_sQ-b_w\left(2+b_s^{\,2}+Q\right)\right)\right)}{\left(-1+\left(b_w-b_s\right)^2\right)^2}+$$
$$4\left(-\frac{1}{-1+\left(b_w-b_s\right)^2}\right)^{3/2}\left(-1+b_w^{\,2}+b_wb_s-2b_s^{\,2}\right)\pi V_s=0. \tag{39}$$

From **Eqns. (38) and (39)**, we obtain two linear equations in two unknowns V_s and Q. These equations are easily solvable to give:

$$V_s=\frac{3\left(b_s-b_w\right)\left(b_s+b_w\right)}{1+\left(b_s-b_w\right)\left(2b_s+b_w\right)},\quad Q=\frac{-1+\left(b_s-b_w\right)^2}{1+\left(b_s-b_w\right)\left(2b_s+b_w\right)}. \tag{40}$$

Taking $b_w=0$ and $b_s=b$, one can retrieve the result presented by **Shack and Lardner [9] and Asghar *et al.* [53]** for a *channel with rigid walls* i.e.

$$V_s=\frac{3b^2}{1+2b^2},\ Q=\frac{-1+b^2}{1+2b^2}. \tag{41}$$

From **Eqn. (40)** it is clear that, swimming speed of the micro-organism in the simplest case of the Newtonian fluid is a function of *undulation amplitude in the micro-organism surface and channel walls*. The only way to externally control the speed of the swimmer is to alter these amplitudes, which is not a reasonable solution. In contrast, for non-Newtonian fluid a strong dependence of propulsive speed is anticipated on different rheological parameters, for instance β, *n and We* which feature in the Carreau model. Thus, in the case of non-Newtonian cervical fluid the *swimming speed can be controlled by the mechanical properties of the fluid*, namely its *viscosity and relaxation time*. These additional features of non-Newtonian fluids provide *an alternative and feasible mechanism for regulating the microorganism swimmer speed without actually changing the parameter of swimming gait*, namely, the undulation amplitude. The Carreau model suggests that enhanced swimming speed can be achieved by tuning the shear-thinning and viscoelastic properties of the cervical mucus. This fact is supported by upcoming figures given in the discussion section.

Proceeding with the analysis, it is necessary to make recourse to a *numerical technique* to calculate V_s and Q since for the non-Newtonian case the afore-mentioned procedure for determining the analytic expression of V_s and Q is not executable due to the highly nonlinear nature of corresponding differential equation for the *Carreau* model. Fundamentally, we have two unknowns V_s and Q which are to be computed from **Eqns. (32), (33)** after computing the stream function $\psi^{\pm}$ for both regions from **Eqn. (28)** subject to boundary conditions **(29) and (30)** for a given set of parameters b_s, b_w, β, We and n. Starting with some initial values of V_s and Q, the boundary value problem corresponding to each region **((28), (29) and (30))** is solved for fixed values of the involved parameters in the domain $h_2 \le y \le h_s$, $h_s \le y \le h_1$, $-\pi \le x \le \pi$ and the resulting computed solution is used to check whether **Eqns. (32) and (33)** are satisfied. If this is attained, the process is terminated, otherwise any root finding algorithm can be employed to refine the values of V_s and Q. For the present computations, we have used the symbolic commercial software **MATLAB** routine **bvp4c** for an efficient numerical solution of the boundary value problem **((28), (29) and (30))** and the modified *Newton-Raphson method* for refining the values of V_s and Q. The process is performed until the absolute error between two consecutive iterative steps is less than 10^{-10}.

5. VALIDATION WITH IMPLICIT FINITE DIFFERENCE METHOD (FDM)

A numerical solution of the boundary value problem consisting of **Eqn. (28)** and boundary conditions **(29) and (30)** provides validation of the **bvp4c** solutions for large values of the rheological parameters. The numerical solution is obtained by employing an implicit iterative finite difference method (**FDM**). We propose the iterative procedure to convert the original nonlinear problem into a linear one at the $(k+1)^{\text{th}}$ iterative step as follows:

$$f^{(k)}\frac{\partial^4\left(\psi^{\pm}\right)^{(k+1)}}{\partial y^4}+\frac{\partial f^{(k)}}{\partial y}\frac{\partial^3\left(\psi^{\pm}\right)^{(k+1)}}{\partial y^3}+\left(\frac{\partial^2 f^{(k)}}{\partial y^2}+H^2\right)\frac{\partial^2\left(\psi^{\pm}\right)^{(k+1)}}{\partial y^2}=0, \qquad (42)$$

$$\left.\begin{array}{l} \left(\psi^{\pm}\right)^{(k+1)}=0, \quad \dfrac{\partial\left(\psi^{\pm}\right)^{(k+1)}}{\partial y}=V_s-1 \\ \dfrac{\partial\left(\psi^{\pm}\right)^{(k+1)}}{\partial x}=0 \end{array}\right\} \begin{array}{l} at\ \ y=h_1=-1+b_w\sin x \\ and\ \ y=h_2=1+b_w\sin x, \end{array} \tag{43}$$

$$\left.\begin{array}{l} \left(\psi^{\pm}\right)^{(k+1)}=\mp Q, \quad \dfrac{\partial\left(\psi^{\pm}\right)^{(k+1)}}{\partial y}=-1 \\ \dfrac{\partial\left(\psi^{\pm}\right)^{(k+1)}}{\partial x}=-b_s\cos x \end{array}\right\} \ at\ \ y=h_s=b_s\sin\left(x+\phi\right), \tag{44}$$

where

$$f^{(k)}\left(y\right)=\beta+\left(1-\beta\right)\left(1+We^2\left(\frac{\partial^2\left(\psi^{\pm}\right)^{(k)}}{\partial y^2}\right)^2\right)^{\frac{n-1}{2}}. \tag{45}$$

Here the superscript (k) indicates the iterative step. It is now clear that the above boundary value problem is linear in $\left(\psi^{\pm}\right)^{(k+1)}$. Inserting finite-difference approximations of $\left(\psi^{\pm}\right)^{(k+1)}$ and its derivative, the boundary value problem comprising **Eqns. (28), (29) and (30)** can be converted into a system of linear algebraic equations and solved for each iterative $(k+1)^{th}$ step. This yields numerical values of $\left(\psi^{\pm}\right)^{(k+1)}$ at each cross-section. The iterative procedure described above is initiated by specifying some suitable initial numerical values of $\left(\psi^{\pm}\right)^{(k+1)}$ at each cross-section. The unknowns V_s and Q are also treated here as missing variables and assigned some starting values. Unfortunately, by increasing the number of iterations a convergent solution is *not always possible*, especially when initial numerical values of $\psi^{\pm}$ are not prescribed carefully. In such circumstances the method of *successive under-relaxation* (SUR) is used. In this method the estimated value of $\psi^{\pm}$ at (k+1) iterative step i.e. $\left(\tilde{\psi}^{\pm}\right)^{(k+1)}$ is refined to achieve the convergent value of $\psi^{\pm}$ at the same step. This can achieved by the following formula:

$$\left(\psi^{\pm}\right)^{(k+1)} = \left(\psi^{\pm}\right)^{(k)} + \tau\left\{\left(\tilde{\psi}^{\pm}\right)^{(k+1)} - \left(\psi^{\pm}\right)^{(k)}\right\}. \tag{46}$$

Here $\tau \in (0,1]$ is an *over-relaxation* parameter. It is also pertinent to select τ as sufficiently small such that convergent iteration is readily attained. The iterations in this problem are carried out to calculate the value of $\psi^{\pm}$ convergent to 10^{-10}. The convergent solution thus obtained is used to verify that **Eqns. (32) and (33)** are satisfied. If the answer is affirmative, this ensures that the correct values of unknowns V_s and Q are achieved. Otherwise, any root-finding method can be used to obtained convergent values of V_s and Q. For the present computations the popular and efficient *Newton-Raphson method* is used. The code for the numerical procedure is developed in **MATLAB**. It is important to mention that this method has earlier been successfully implemented by **Ali *et al.* [33] and Asghar *et al.* [38]** in the context of gliding motility of bacteria and swimming spermatozoa showing excellent accuracy and stability. The results obtained via this hybrid numerical method are depicted via superimposed blue filled dots in **Figs. 2-5**. Clearly, there is an excellent correlation between the results predicted by both methods. This testifies to the validity of the hybrid numerical technique-based results presented in subsequent section and confidence in the current simulations is therefore justifiably high.

6. RESULTS AND DISCUSSION

In this section the computational results are shown graphically in **Figs. 2-10** and discussed in detail.

6.1 SPEED OF MICROSWIMMER AND FLOW RATE OF CARREAU FLUID

For specific values of one of the key rheological parameters, namely *Weissenberg number (We)*, the pairs V_s and Q can be readily obtained from the aforementioned numerical procedure. These pairs when substituted in **Eqn**. **(35)** furnish the corresponding values for the *rate of work done* by the spermatozoa.

In **Fig. 2,** the swimming speed of the micro-organism in both shear-thinning $(n = 0.65)$ and shear-thickening $(n = 1.35)$ fluid as a function of Weissenberg number (We) is shown for six different values of Hartmann number (H). Propelling speed in case of passive channel $(b_w = 0)$ is

displayed in **Fig. 2(a)** for two different undulation amplitude (b_s). On the other hand, organism speed for two different active channel case i.e. $b_w < b_s$ and $b_w > b_s$ with two different phase difference (ϕ) and viscosity ratio (β) is expounded in **Fig. 2(b)** and **(c)**, respectively.

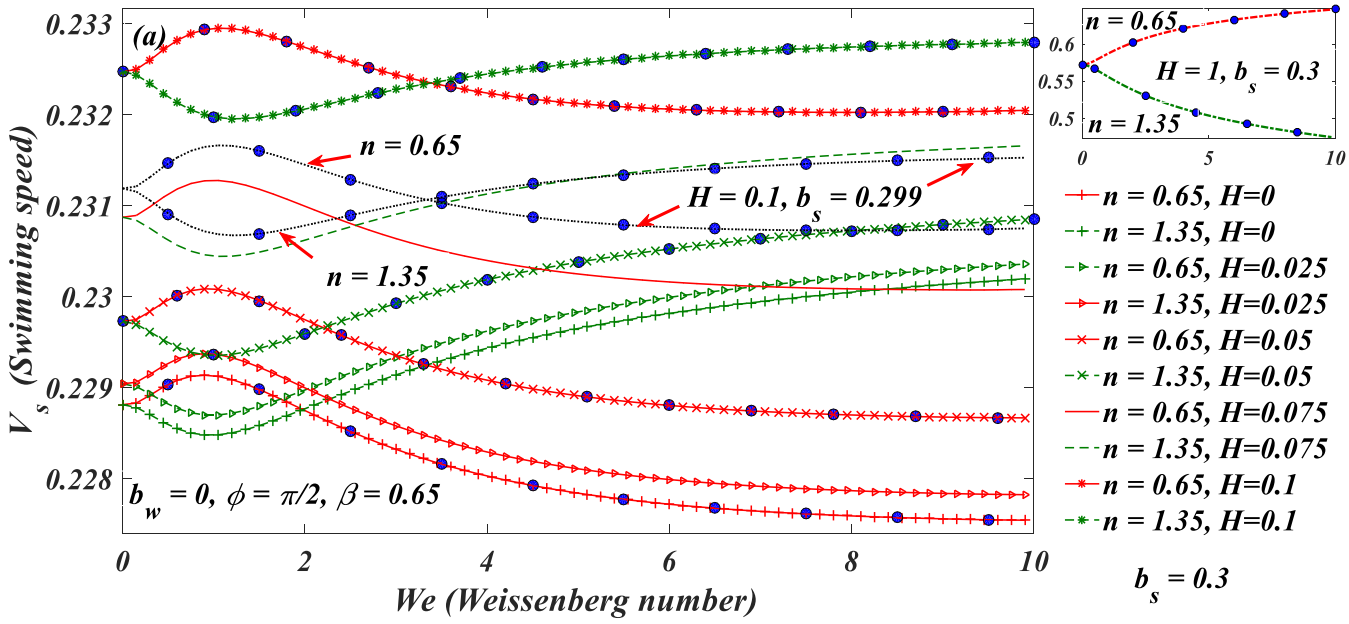

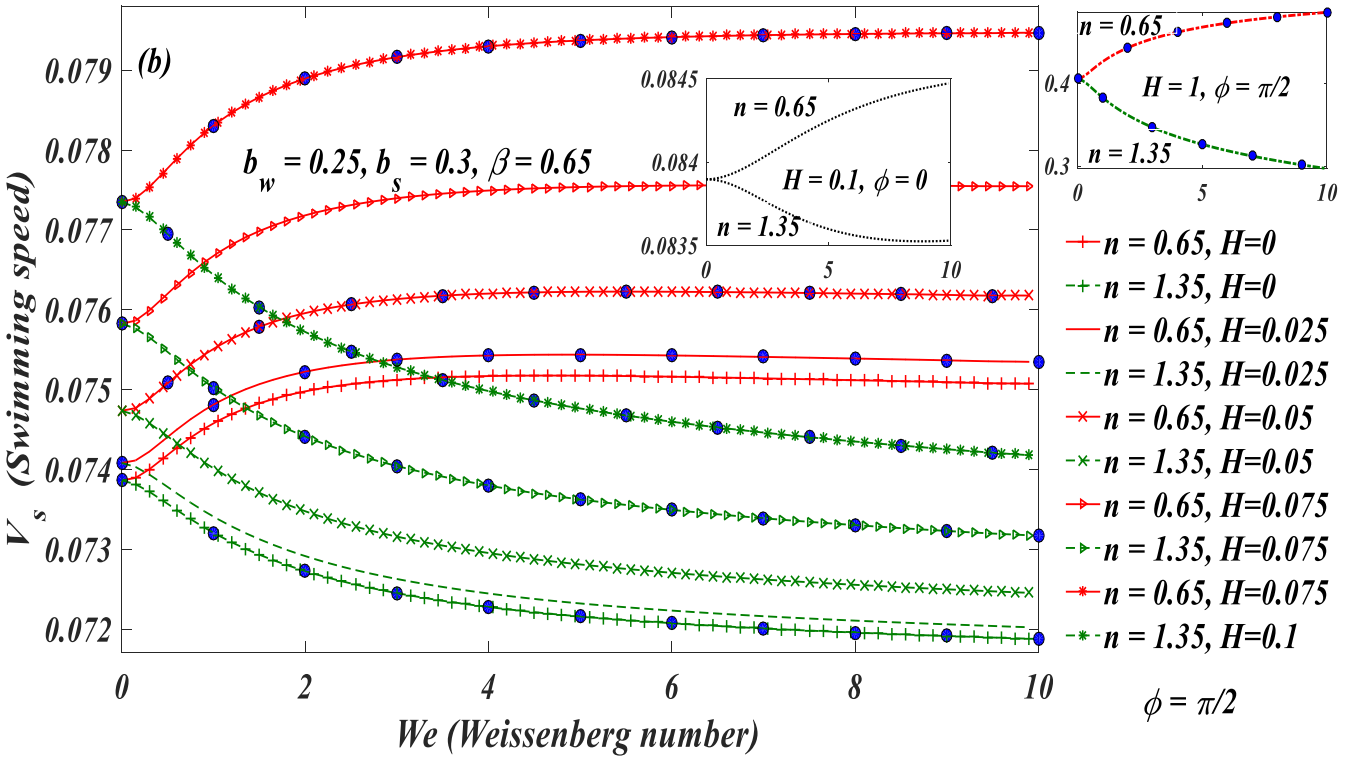

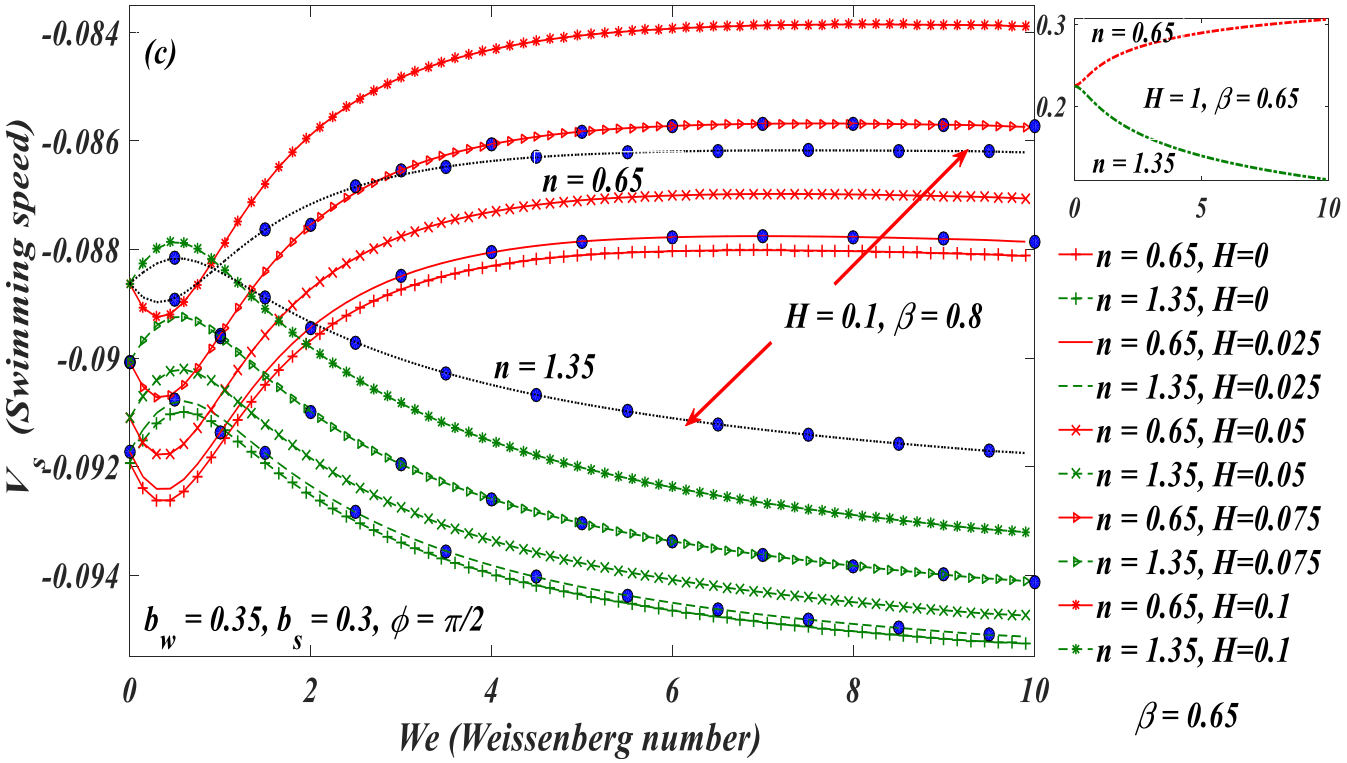

Fig.2. Speed of micro-swimmer in passive and active channel against Weissenberg number with different magnetic field strengths, mucus rheology, phase difference and udulation amplitude.

In **Fig. 2(a),** for shear-thickening case, it can be observed that the speed slightly decreases, attains a minimum and thereafter exhibits an increasing trend with increasing Weissenberg number. However, this increase is not significant for larger Weissenberg number. In fact, it is very slow and as a result the profiles assume a plateau-type topology. For relatively greater magnetic field strength $(H=1)$ the micro-swimmer pushes itself with greater speed. The above observations clearly highlight the assisting nature of magnetic field in the swimming hydrodynamics of spermatozoa when the surrounding liquid is of shear-thickening nature. However a converse trend is witnessed for a micro-swimmer propelling through shear-thinning mucus. One can also witness a reduction in swimming speed with small amplitude (b_s).

Fig. 2(b) is plotted for an active cervical canal with wall undulation less than organism undulation i.e. $b_w(=0.2) < b_s(=0.3)$. In comparison to **Fig. 2(a),** which is plotted for straight channel, the spermatozoa slow down due to the wavy cervical walls. This resistance to the swimming speed is due to the narrow passage of the active cervical canal, while in case of passive walls the channel

is comparatively wider. This fact can be observe in the upcoming figures (**Fig. 9(a)-(f)**). It can also be perceived from **Fig. 2(b)** that the speed of the organism exhibit a uniform (monotonic) increasing behavior for shear-thinning case and a converse trend is observed for shear-thickening liquid. Moreover, (by comparing corresponding curves for $H = 0.1$) the organism possessing synchronized wave $(\phi = 0)$ with the cervical channel wave, can swim faster as compared to the non-synchronized organism $(\phi = \pi / 2)$.

Fig. 2(c) illustrates the swimmer's propelling speed for an active cervical canal with wall's wave amplitude greater than swimmer's wave amplitude i.e. $b_w(=0.4) > b_s(=0.3)$. With reference to **Fig. 2(b),** a relatively greater magnitude of swimming speed is witnessed in **Fig. 2(c)** but in the opposite direction (positive *x-axis*). This means that the travelling cervical waves with higher undulating amplitude then swimmer's undulation, causes the organism to propel along with them (in their direction of propagation). The shear-thinning rheology of the surrounding fluid and higher magnetic field reduce this reverse propulsion and encourages the micro-swimmer to swim faster in the negative x-direction. While increasing viscosity ratio $(\beta \longrightarrow 1)$ leads to the *Newtonian* case. Further, interpretation of these profiles indicates that increasing amplitude of wave in the channel walls and increasing phase difference between organism and channel waves play a resistive role to swimming speed. This is clearly discouraging for swimming microorganisms. Thus, for passive channel, a *magnetic shear-thinning medium with small* Weissenberg number $(0 \le We \le 1)$ and *magnetic shear-thickening medium with large* Weissenberg number $(We > 1)$ are the most scenario suitable for swimming micro-organism. For active channel, greater magnetic field strength, undulation amplitude in swimmer surface, shear-thinning with large Weissenberg number $(We > 5 \text{ or } 10)$ and low phase difference leads to faster propulsion of swimming spermatozoa.

In **Fig. 3,** a comparison of flow rate of cervical mucus against Weissenberg number for both active and passive cervical channel is presented. **Figs. 3(a)-(c)** are exactly plotted for same set of b_w, b_s, β, H, ϕ *and* n as used in **Figs. 2(a)-(c),** respectively.

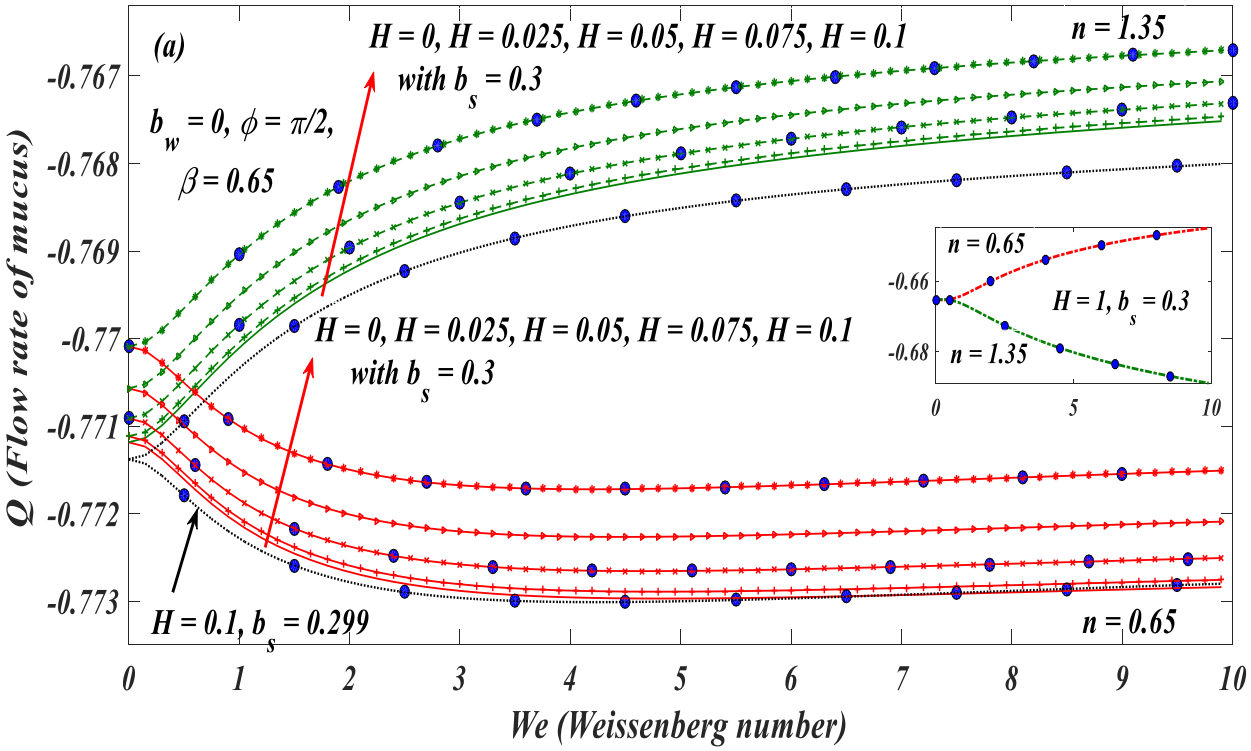
(a)
H = 0, H = 0.025, H = 0.05, H = 0.075, H = 0.1
with b_s = 0.3
n = 1.35
b_w = 0, ϕ = π/2,
β = 0.65
H = 0, H = 0.025, H = 0.05, H = 0.075, H = 0.1
with b_s = 0.3
n = 0.65
H = 1, b_s = 0.3
n = 1.35
H = 0.1, b_s = 0.299
n = 0.65
Q (Flow rate of mucus)
We (Weissenberg number)

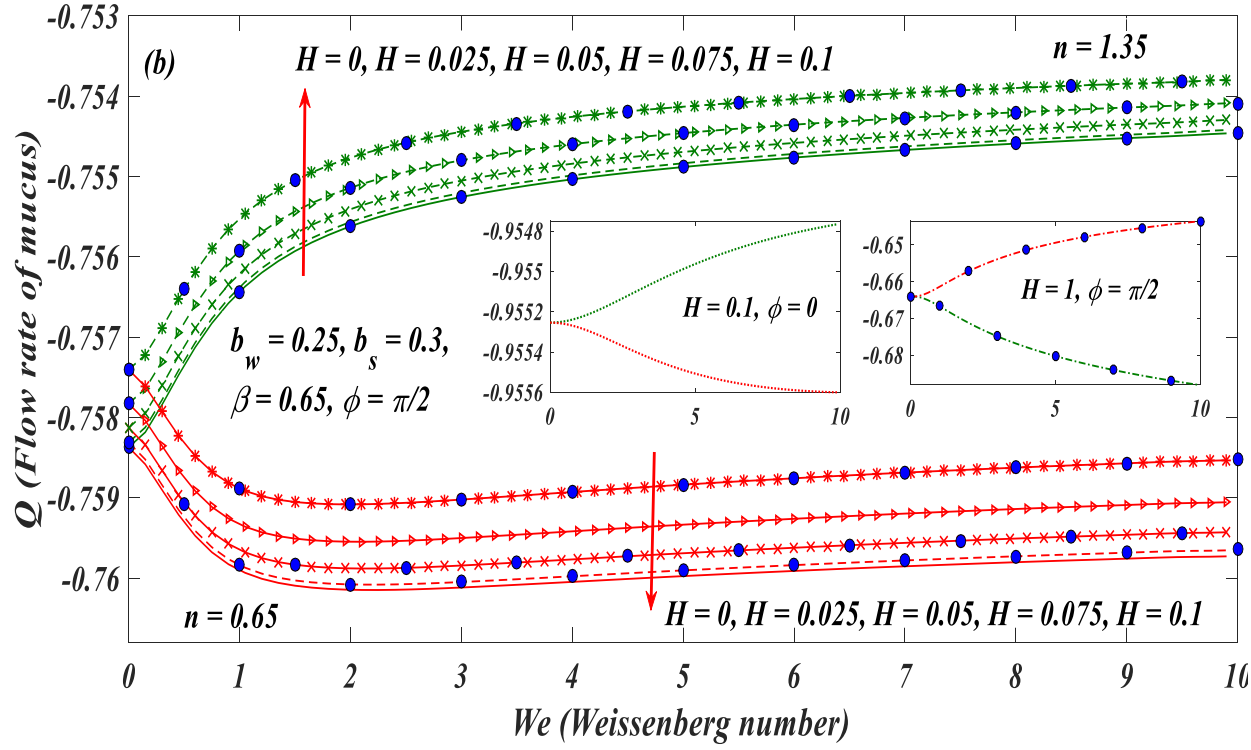
(b)
H = 0, H = 0.025, H = 0.05, H = 0.075, H = 0.1
n = 1.35
b_w = 0.25, b_s = 0.3,
β = 0.65, ϕ = π/2
H = 0.1, ϕ = 0
H = 1, ϕ = π/2
n = 0.65
H = 0, H = 0.025, H = 0.05, H = 0.075, H = 0.1
Q (Flow rate of mucus)
We (Weissenberg number)

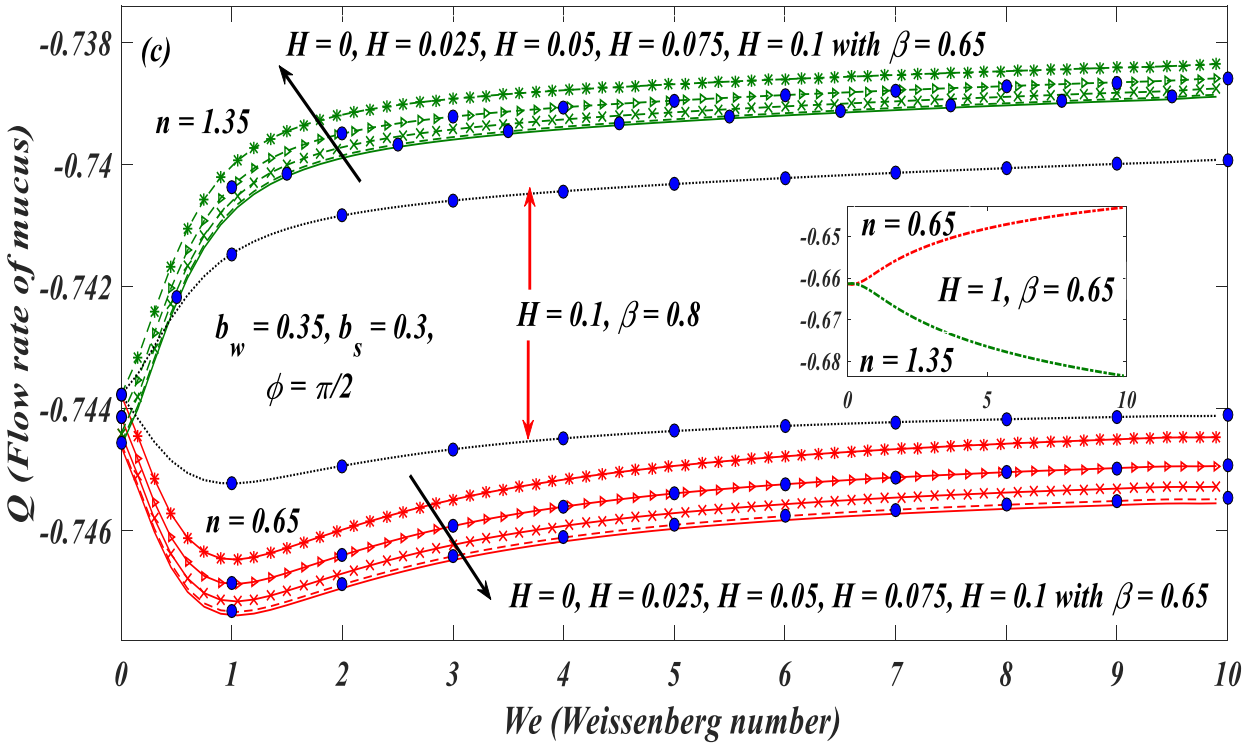

Fig.3. Flow rate of cervical fluid in passive and active channel against Weissenberg number with different magnetic field strengths, mucus rheology, phase difference and udulation amplitude.

For both active and passive wall vicinity the magnitude of the flow rate increases with increasing Hartman number for *shear-thinning* mucus $(n<1)$. Small undulation in the swimming sheet and synchronization between the (organism/canal) waves also assist the flow rate for the said case. However, the opposite trend is computed for *shear-thickening* cervical liquid. In comparison to **Fig. 3(a)**, wavy channel case as shown in **Fig. 3(b)** and **(c)** reduces the flow rate of the cervical fluid. It is deliberately shown that flow rate is a decreasing function of Weissenberg number for shear-thickning fluid, however in case of shear-thinnning fluid, flow rate initially increases (in magnitude) with Weissenberg number and after reaching a critical point $(We=1)$ there is a marginal reduction in flow rate. It is also anticipated that for greater values of Weissenberg number i.e. $We>10$ both the swimming speed and flow rate exhibit an asymptotic behavior.

6.2 RATE OF WORK DONE AT DIFFERENT SWIMMING SPEED

For both active and passive channel the rate of work done corresponding to different propulsive speeds and flow rates (shown in **Figs. 2 and 3)** as a function of Weissenberg number (We) for six different values of Hartmann number (H) and two different undulation amplitude (b_s), phase difference (ϕ) and viscosity ratio (β) is depicted in **Fig. 4**. For brevity, here we show the shear-thinning case $(n<1)$ only and we anticipate that the shear-thickening case leads to a converse trend in the energy losses.

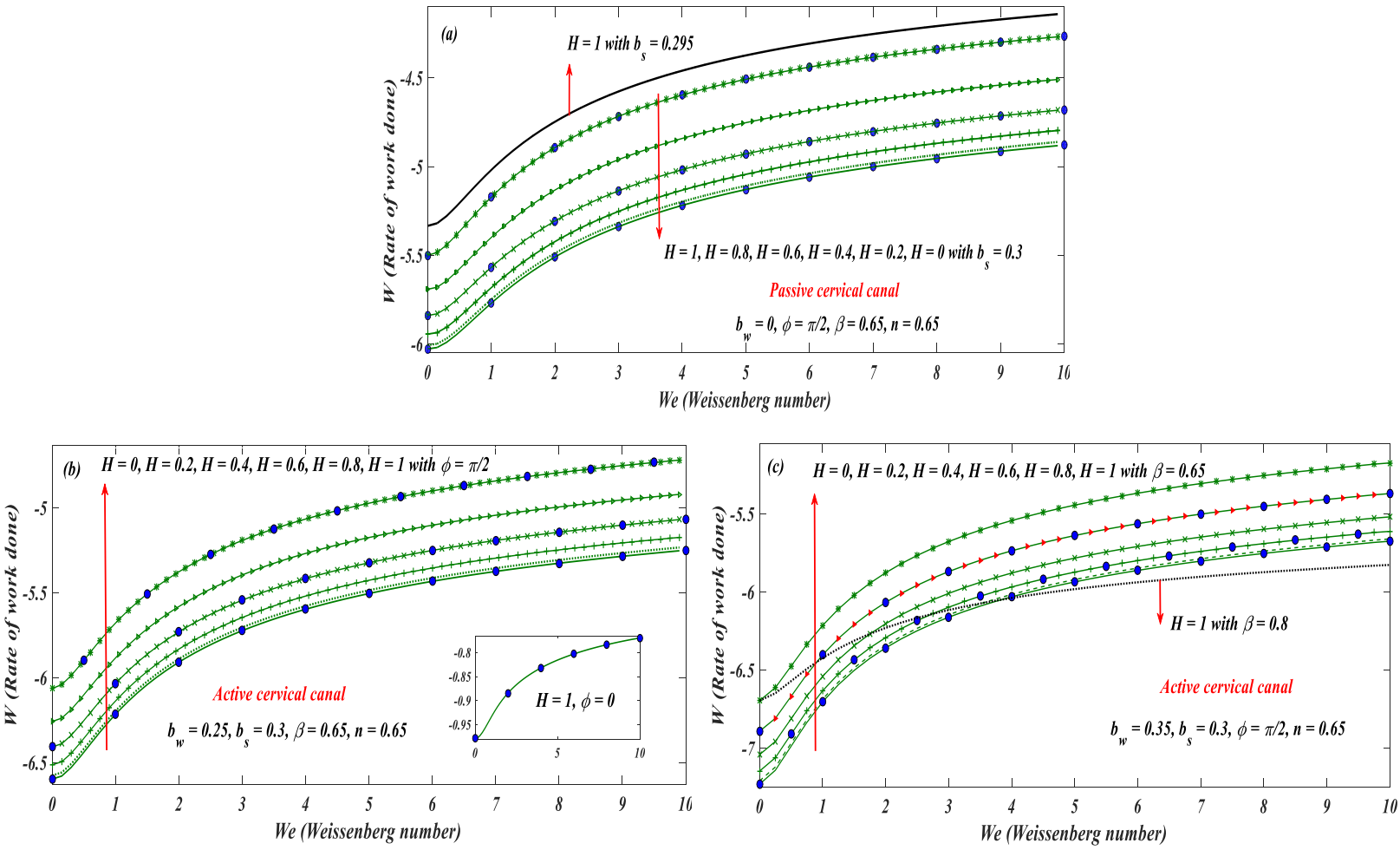

Fig.4. Rate of workdone against Weissenberg number in passive and active channel with different magnetic field strengths, mucus rheology, phase difference and udulation amplitude

It is observed from **Fig. 4(a)** and **(b)** that the rate of work done exhibits a qualitatively increasing trend with increasing Weissenberg number and Hartmann number for shear-thinning fluid. **Fig. 4(c)**, **(**corresponding to **Fig. 2(c)** which is plotted for $b_w > b_s$ showing a reverse propulsion of the organism**)** reveals that there is a greater loss of energy as compared to other two cases. This energy loss reduces with increasing Weissenberg number and Hartmann number. This figure also authenticates that a synchronized swimmer expanded less energy as compared to a non-synchronized swimmer and same fact is true for large amplitude swimmers.

6.3 COMPARISON OF ENERGY EXPENDED AT SAME SWIMMING SPEED

In the above figures (**Figs. 4),** the *rate of work done* is computed corresponding to different propulsive speeds. If the spermatozoa is somehow able to maintain the same swimming speed in two different scenarios, then it will be more appropriate to compare its power dissipation in both cases. The same swimming speed in two different circumstances can be obtained by altering wave amplitude in the micro-swimmer surface. One scenario could be the spermatozoa swimming in an *active channel with specified speed in the presence of magnetic field* while another scenario may entail the *same micro-organism swimming with the same specified speed through an active channel in the absence of magnetic field*. The comparison can also be made on the basis of activeness or passiveness of the channel and rheology of the surrounding fluid. All these cases are shown here in **Figs. 5-7** in the form of histograms.

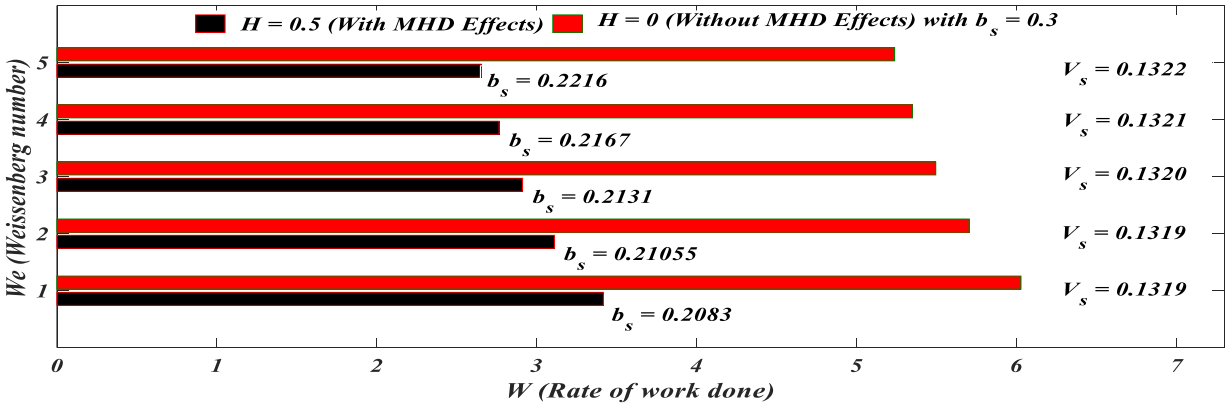

Fig. 5. Comparison of energy expanded by the organism swimming through Carreau liquid with and without MHD effects with same propulsive speed. With $n = 0.75, b_w = 0.2, \phi = \pi/2$ *and* $\beta = 0.5$

Fig. 5 corresponds to the first case. It is observed that application of magnetic field reduces the energy expanded by the micro-organism i.e. less amount of work is required by the micro-organism to maintain the same speed in a magnetohydrodynamic environment.

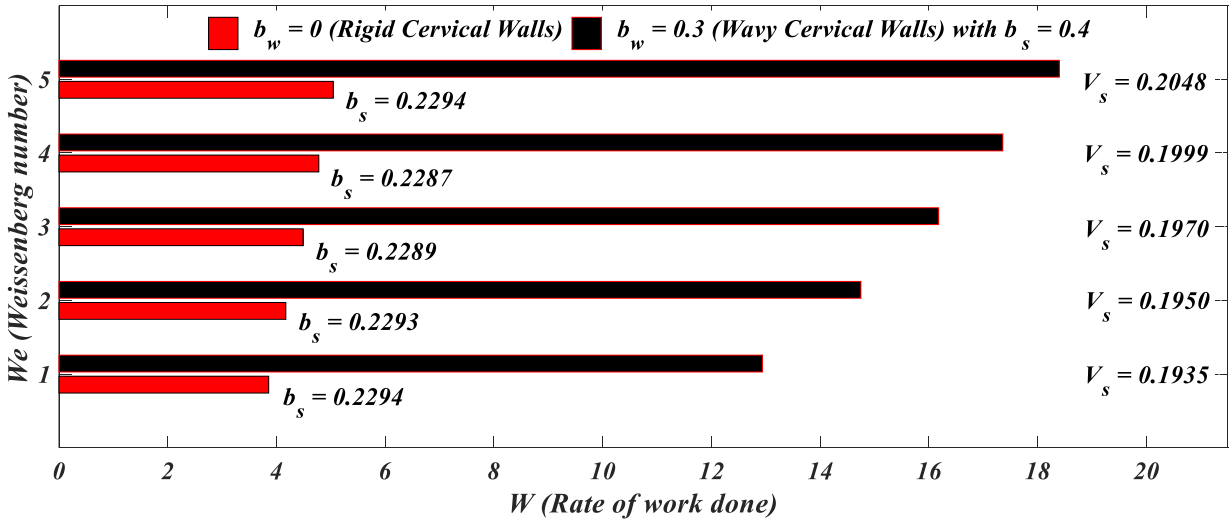

Fig.6. Comparison of energy expanded by the organism swimming through active and passive channels with same propulsive speed. With $n = 1.35, H = 0.4, \phi = \pi/2$ *and* $\beta = 0.4$.

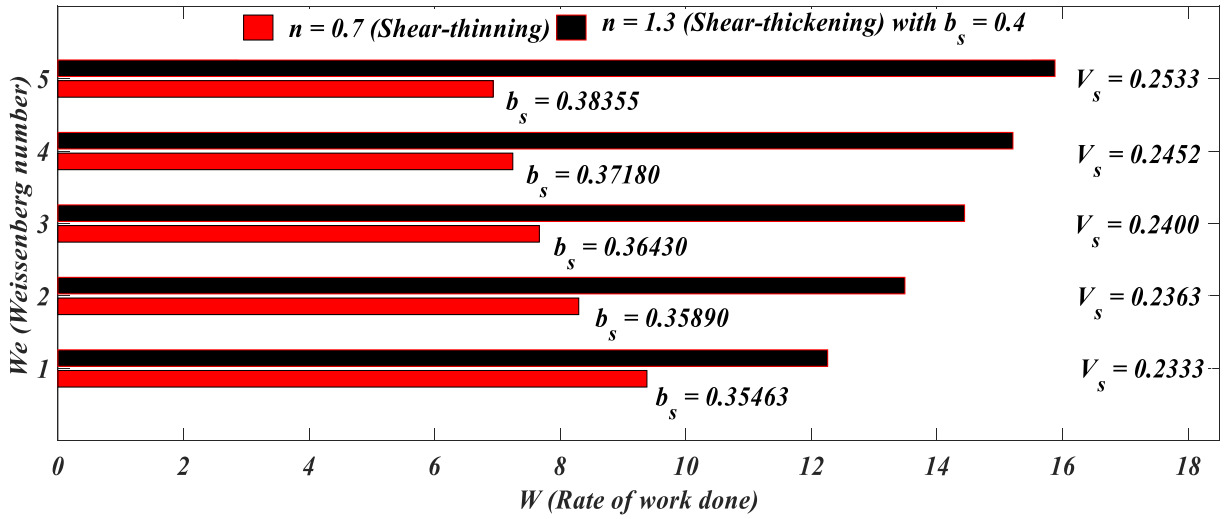

Fig. 7. Comparison of energy expanded by the organism swimming through shear-thickening and shear-thinning liquid with same propulsive speed. With $b_w = 0.3, H = 0.6, \phi = \pi/2$ *and* $\beta = 0.5$

Fig. 6 reveals that activeness of the channel increase the energy losses substantially. In other words, *energy expended by the micro-organism moving with the specified speed in a passive channel is substantially less than the corresponding energy expanded by the micro-organism moving with the same speed in an active channel*.

Fig. 7 highlights that the energy losses can also be controlled by adjusting the rheology of the surrounding liquid. In this regard it is observed that the *shear-thinning* characteristic is quite favorable to achieve the required goal.

6.4 STREAM LINES OF THE MAGNETIC CERVICAL LIQUID FLOW

From the above discussion, it is clear that there are *four different ways* to control the speed of swimming sheet. These are: (1) by disturbing synchronization between the waves present in swimming sheet and channel walls, (2) by varying the applied magnetic field, (3) by altering wave amplitude of the organism surface or channel walls, (4) by tuning the mucus rheology present between the spermatozoa and cervical canal.

A comparison of streamline patterns of cervical mucus for different phase difference, magnetic field strengths, occlusions in spermatozoa surface, fluid rheology, rigid and active cervical channels is shown through **Figs. 8-10.** In **Fig. 8,** the parameters b_s, b_w, H, We, n *and* β are kept constant throughout for the active channel and **plots (a)-(d)** are produced by varying the phase difference between the micro-swimmer and channel waves.

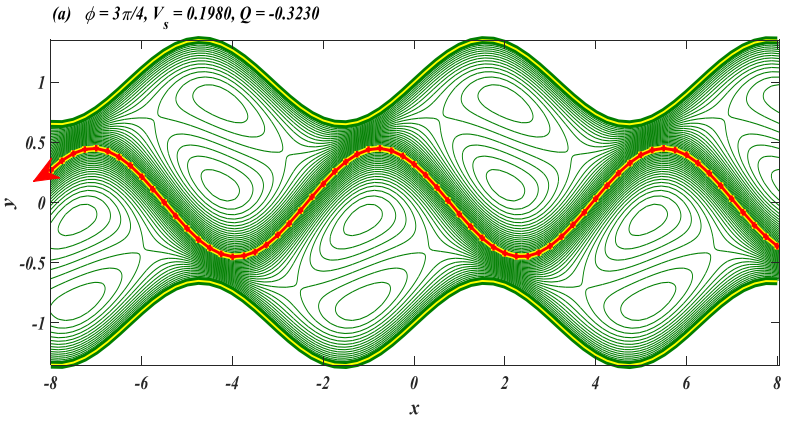

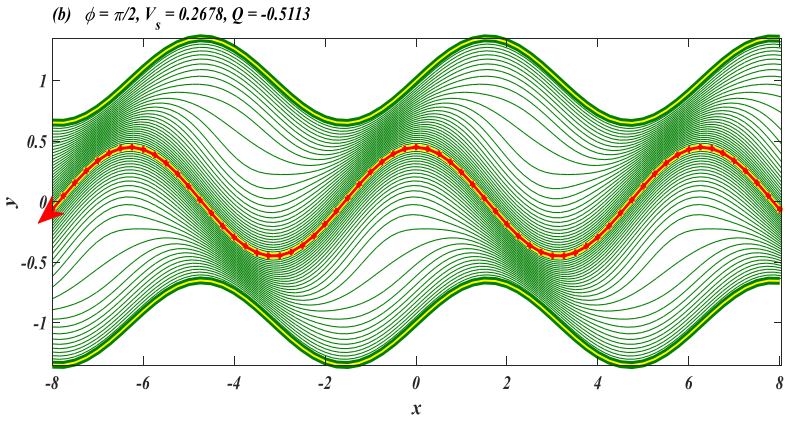

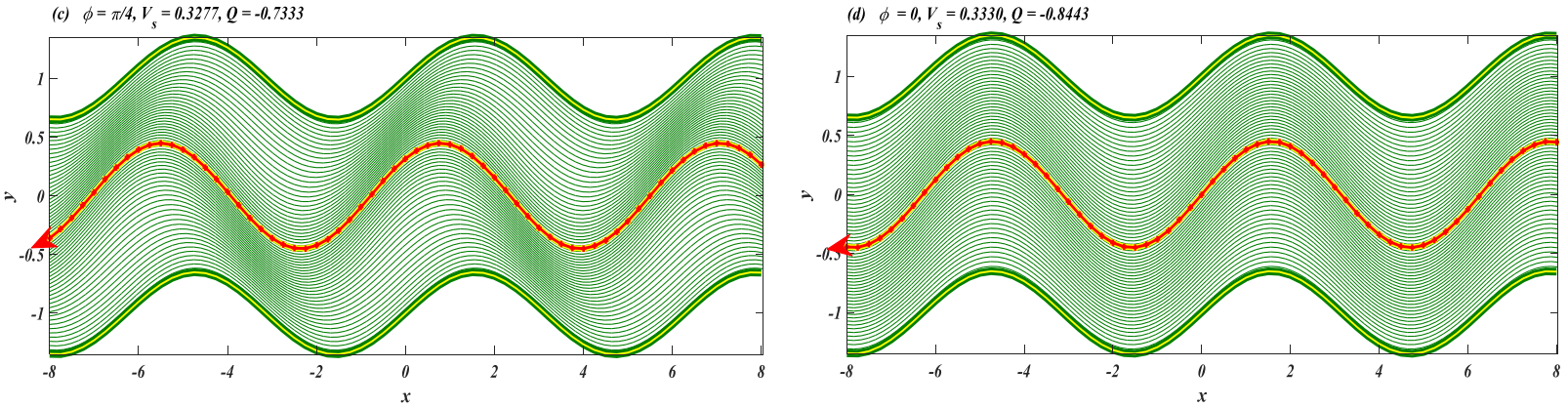

Fig. 8. Streamline of flow in an active channel with different pairs of swimming speed V_s, flow rate Q and phase difference ϕ with $b_s = 0.45$, $b_w = 0.35$, $H = 0.5$, $We = 7$, $n = 0.5$ *and* $\beta = 0.55$.

The red-yellow colored undulating curve in the middle of the channel specifies the swimming micro-swimmer trajectory. The corresponding streamlines near the cervical walls and swimmer surface resemble this trajectory in geometric shape, which is of the form of a sinusoidal wave. For *the non-synchronized wave scenario* (with phase difference $\phi = 3\pi/4$) the numerical computations yield $V_s = 0.1980$ *and* $Q = -0.3230$ as shown in **plot 8(a).** The recirculating zones appear in the channel both below and above the micro-organism swimmer surface, which are anticipated to be reduced as the organism swims faster while approaching the synchrony. This fact can be observed in **plot 8(b)** in which the speed becomes $V_s = 0.2678$ with comparatively smaller phase difference i.e. $\phi = \pi/2$. There are also a few minor void regions without any trapped bolus. With further smaller phase difference physically the case when the swimmer is in phase with the channel is approached. In such a case (**plots 8 (c) and (d)**) the corresponding streamlines are closely packed sinusoidal shape curves spanning the entire channel. In both **plots 8 (c) and (d)** there is no evidence of recirculating zones nor any kind of void regions in any part of the channel.

The assessment of level curves representing the cervical liquid (Carreau fluid) around the spermatozoa for both rigid and active cervical channels with different magnetic field strengths (as simulated via the Hartmann number, *Ha*) are depicted in **Figs. 9(a)-(f).** By keeping fluid rheology and organism amplitude $(b_s = 0.4)$ fixed, **plots (a) and (b)** are displayed for the passive channel $(b_w = 0)$, while **plots (b)-(f)** are displayed for the active channel $(b_w = 0.3$ and $b_w = 0.5)$ for two different Hartman numbers. Referring to **plots (a) and (b),** the level curves near the rigid walls are

straight lines and they adopt the shape of the swimmer in close vicinity of the swimming sheet. Comparison of **plots (a) and (b),** reveals a decrease in the number of streamlines with increasing Hartman number or swimming speed. The wavy channel (canal) significantly reduces the propelling velocity and increases the intensities of fluid streamlines near the undulating organism and channel walls (as shown in **plots (c) and (d)**). This situation creates a circulating zone in the corresponding cross sections for both the upper and lower part of the channel (as shown in **plot (c)** with no magnetic field). However, inspection of **plot (d)** indicates that with magnetic effects these circulating zones disappear and the result is a void region.

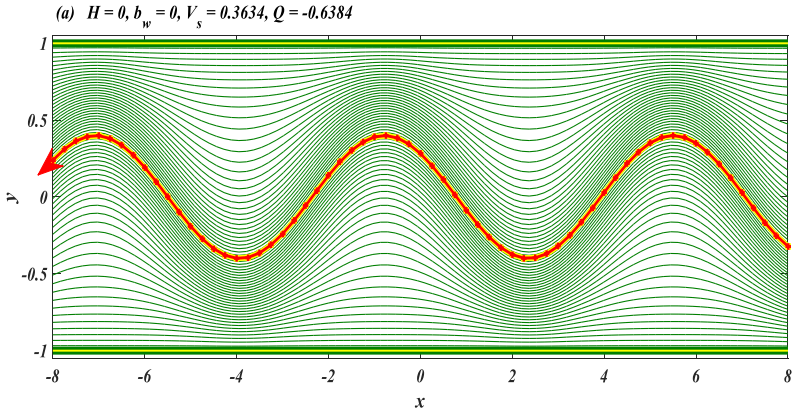

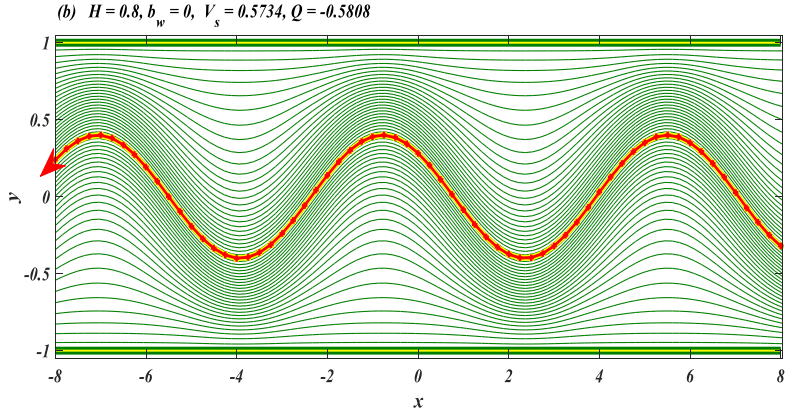

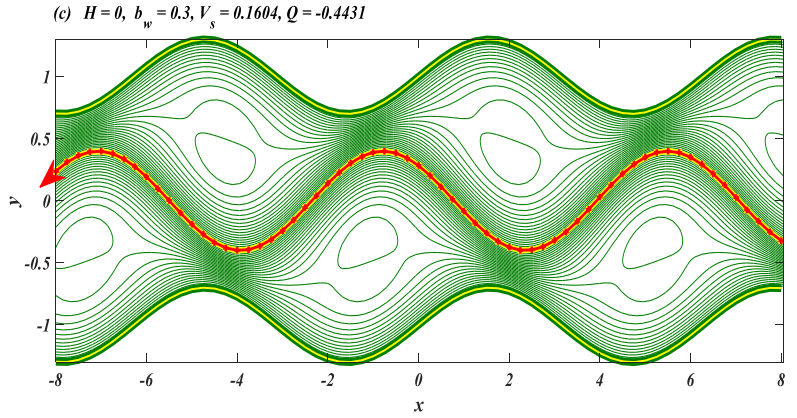

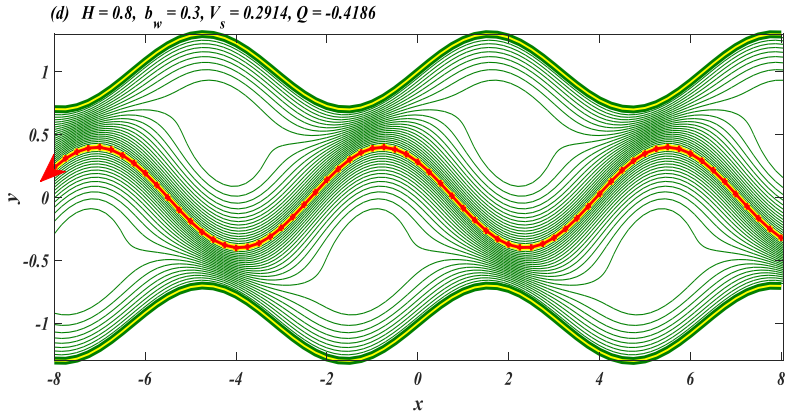

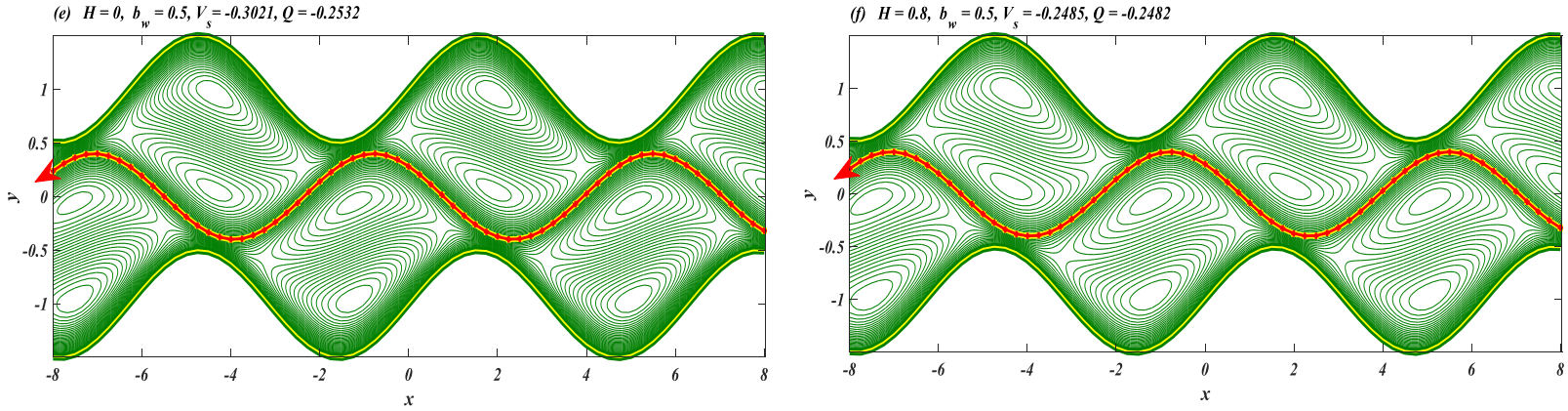

Fig. 9. Streamline of flow in passive and active channels with different pairs of swimming speed V_s, flow rate Q and Hartman number H with $b_s = 0.4$, $We = 5$, $n = 0.7$, $\beta = 0.65$ *and* $\phi = 3\pi/4$.

Finally, **plots (e) and (f)** expounded the case in which there is a large amplitude of waves in the channel walls as compared to the micro-swimmer organism, which leads to reverse propulsion ("back-swimming") of the organism. The speed of spermatozoa is significantly higher (in magnitude) in comparison with the case of small amplitude wavy walls. It can be clearly witnessed that the number of circulating zones is significantly increased i.e. there is substantial intensification in the recirculation and vortex structures. Furthermore, a comparison of **plots (e) and (f)** reveals that the presence of magnetic field encourages faster swimming whereas it reduces the *number* of circulating zones.

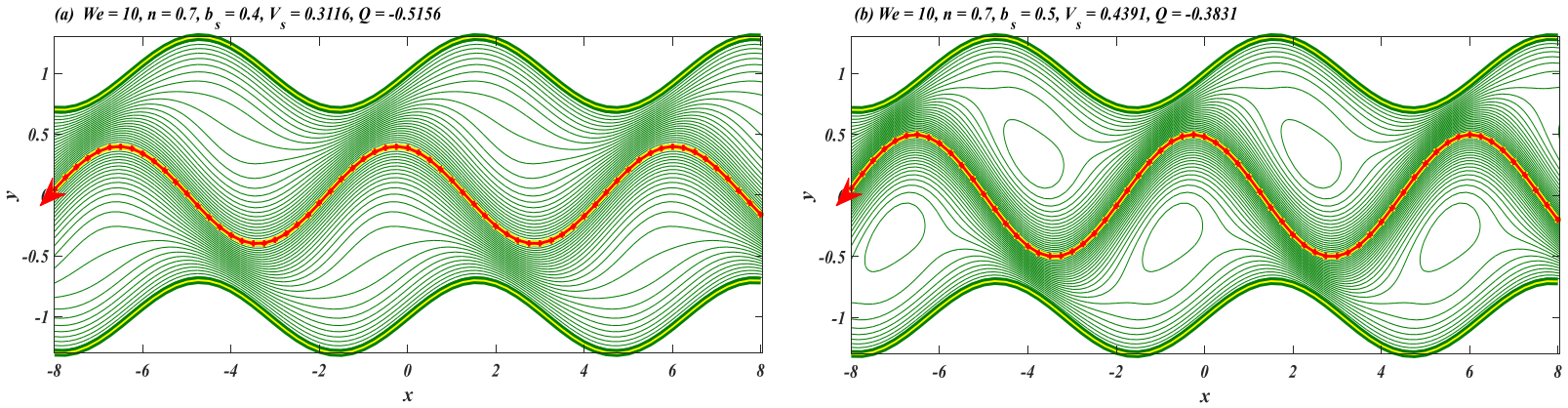

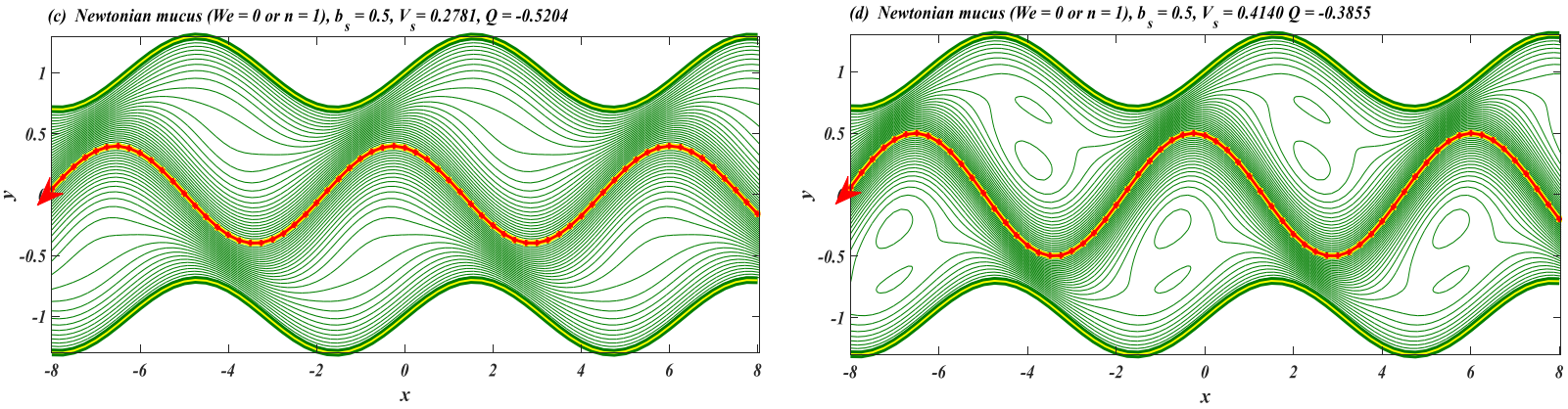

Fig.10. Streamline patterns of the fluid in wavy channel with different pairs of rheological parameters and swimming gait $b_w = 0.3,\ H = 0.7,\ \beta = 0.6$ *and* $\phi = 7\pi/12$.

Figs. 10(a)-(d) are plotted by tuning the fluid rheology i.e. by adjusting *We*, *n* and β and micro-swimmer organism undulation i.e. by varying b_s. Of course, the amplitude of wave in spermatozoa surface cannot be controlled externally. Nevertheless, the present computations are not limited to living micro-organisms only but equally valid for artificially designed magnetic micro-swimmers. From **Figs. 10** it is clearly observed that the strength of streamlines decreases in corresponding middle regions of both halves of the channel as the swimming speed increases.

7. CONCLUSIONS

The two-dimensional hydrodynamic propulsion of a micro-organism (spermatozoa) swimming through an active channel filled with hydromagnetic Carreau fluid under static transverse magnetic field, as a simulation of cervical magnetic field therapy in embryological medicine, is explored. Taylor's wavy sheet model with phase shift is deployed for the micro-organism and sinusoidal waves are imposed at the channel walls. The differential equation describing the problem is developed by invoking the low Reynolds number and long wavelength approximations. A numerical scheme based on the symbolic software **MATLAB** routine **bvp-4c** is used to compute the micro-organism velocity and flow rate for large values of rheological parameters. The results obtained via **bvp-4c** are validated with an alternative *implicit finite difference numerical scheme* ***(*FDM*).*** The dependence of the rate of work done by the swimming micro-organism on different

rheological parameters is also elucidated. The key findings emerging from the current theoretical analysis may be summarized as follows:

- The application of constant applied magnetic field proves to be an assistive factor in swimming propulsion and aids the micro-swimmer (organism) locomotion, while activeness of the channel inhibits the propulsion of micro-swimmers.
- The swimming speed achieve maximum/minimum magnitudes at a certain value of Weissenberg number for thinning/thickening fluid under the action of magnetic field (Hartmann number) for the passive channel, while the speed increases/decreases uniformly with increasing Weissenberg number for thinning/thickening fluid in the case of an active channel.
- Larger amplitude in the micro-swimmer (e.g. representing sperm flagella) enhances the swimming speed of the micro-organism and less energy is utilized in this case.
- If the micro-organism is made to swim through both passive and active channels with the same speed, then the energy consumed is lower in the former case. Similarly, if the organism is made to swim through both hydromagnetic (*Hartmann number* > 0) and hydrodynamic (*Hartmann number* = 0) biofluid environments with the same speed, then the energy consumed is also lower in the former case Thus, swimming is *energy-efficient* in a *passive channel* with a *magnetohydrodynamic* biofluid environment.
- The strength of recirculating zones and streamlines appearing in the corresponding central regions of upper and lower halves decreases with faster propulsion.

The current study has considered micro-organism propulsion via wavy sheet swimming in *biorheological magnetohydrodynamic* fluids. Future works will consider propulsion in electro-rheological fluids under the action of axial electrical fields [**49-50**] and additionally may also be generalized to consider simultaneous electrical and magnetic fields [**51**] and more complex rheological constitutive models e.g. electro-viscoelastic fluids [**52**] which are also of relevance to electro/magnetic cervical and other medical treatments. The hybrid numerical procedure developed in the current article offers considerable potential in these new exciting areas.

REFERENCES

[1] G. I. Taylor, Analysis of the swimming of microscopic organisms. *Proc. R. Soc. Lond. A,* **209** (1951) 447-461.

[2] G. I. Taylor, The action of waving cylindrical tails in propelling microscopic organisms. *Proc. R. Soc. Lond. A,* **211** (1952) 225-239.

[3] G. J. Hancock, The self-propulsion of microscopic organisms through liquids. *Proc. R. Soc. Ser.*, ***A*217** (1953) 96–121.

[4] J. Gray and G.J. Hancock, The propulsion of sea-urchin spermatozoa. *J. Exp. Biol.,* **32** (1955) 802 -814.

[5] J. E. Drummond, Propulsion by oscillating sheets and tubes in a viscous fluid. *J. Fluid Mech*., **25** (1966) 787-793.

[6] A. J. Reynolds, The swimming of minute organisms. *J. Fluid Mech*., **23** (1965) 241-260.

[7] E. O. Tuck, A note on swimming problem. *J. Fluid Mech*., **31** (1968) 305-308.

[8] W. J. Shack and T. J. Lardner, A long wavelength solution for a microorganism swimming in a channel. *Bull. Math. Biol*., **36** (1974) 435-444.

[9] D. F. Katz, On the propulsion of micro-organisms near solid boundaries. *J. Fluid Mech*., 64 (1974) 33-49.

[10] J. B. Shukla, B. R. P. Rao and R. S. Parihar, Swimming of spermatozoa in cervix: effects of dynamical interaction and peripheral layer viscosity. *J. Biomech*., 11, (1978) 15–19.

[11] R. E. Smelser, W. J. Shack and T. J. Lardner, The swimming of spermatozoa in an active channel. *J. Biomech*., **7** (1974) 349–355.

[12] J. B. Shukla, P. Chandra and R. Sharma, Effects of peristaltic and longitudinal wave motion of the channel wall of movement of micro-organisms: application to spermatozoa transport. *J. Biomech.,* **21** (1988) 947–954.

[13] G. Radhakrishnamacharya and R. Sharma, Motion of a self-propelling micro-organism in a channel under peristalsis: effects of viscosity variation. *Nonlinear Anal. Model.,* **12** (2007) 409–418.

[14] A. Walait, A. M. Siddiqui and M. A. Rana, Analysis of a self-propelling sheet with heat transfer through non-isothermal fluid in an inclined human cervical canal. *J. Biol. Phys*, (2018) https://doi.org/10.1007/s10867-018-9481-z.

[15] T. K. Chaudhury, On swimming in a viscoelastic liquid. *J. Fluid Mech*., **95** (1979) 189-197.

[16] L.D. Sturges, Motion induced by a waving plate, *J. Non Newton Fluid Mech.*, **8** (1981) 357–364.

[17] M. Sajid, N. Ali, O. Anwar Bég, A.M. Siddiqui, Swimming of a singly flagellated micro-organism in a magnetohydrodynamic second order fluid. *J. Mech. Med. Biol.*, **17** (2017) 1750009.

[18] E. Lauga, Propulsion in a viscoelastic fluid. *Phys. Fluids,* **19** (2007) 083104.

[19] M. Sajid, N. Ali, A.M. Siddiqui, Z. Abbas and T. Javed, Effects of permeability on swimming of a micro-organism in an Oldroyd-B Fluid. *J Porous Media*, **17** (2014) 59–66.

[20] N. Ali, M. Sajid, Z. Abbas and O. Anwar Bég, Swimming dynamics of a micro-organism in a couple stress fluid: a rheological model of embryological hydrodynamic propulsion. *J. Mech. Med. Biol.*, **17** (2017) 1750054.

[21] P. Sinha, C. Singh and K.R. Prasad, A microcontinuum analysis of the self-propulsion of the spermatozoa in the cervical canal, *Int .J. Engng. Sci.*, **20** (1982) 1037-1048.

[22] D. Philip and P. Chandra, Self-propulsion of spermatozoa in microcontinua: effects of transverse wave motion of channel walls. *Arch. Appl. Mech*., **66** (1995) 90-99.

[23] N. J. Balmforth, D. Coombs and S. Pachmann, Microelastohydrodynamics of swimming organisms near solid boundaries in complex fluids. *Q. J. Mech. Appl. Math*., **63** (2010) 267-294.

[24] T. R. Ives and A. Morozov, The mechanism of propulsion of a model micro-swimmer in a viscoelastic fluid next to a solid boundary, *Phys. Fluids,* **29** (2017) 121612.

[25] F.A. Morrison, *Understanding Rheology*. Oxford University Press Inc, New York, USA (2001).

[26] J. R.Vélez-Cordero, E. Lauga, Waving transport and propulsion in a generalized Newtonian fluid. *J. Non-Newtonian Fluid Mech*., **199** (2013) 37–50.

[27] T. Hayat, M. Iqbal, H. Yasmin, F. Alsaadi and N. Alotaibi, Nonlinear peristaltic flow of a Carreau fluid in the presence of Hall current and convective effect, *Eur. Phys. J. Plus* **129** (2014) 107.

[28] T. Hayat, S. Farooq, A. Alsaedi and B. Ahmad, Hall and radial magnetic field effects on radiative peristaltic flow of Carreau-Yasuda fluid in a channel with convective heat and mass transfer. *J. Magn. Magn. Mater.,* **412** (2016) 207-216.

[29] T. Hayat, S. Farooq, B. Ahmad and A. Alsaedi, Characteristics of convective heat transfer in the MHD peristalsis of Carreau fluid with Joule heating. *AIP Advances*, **6** (2016) 045302.

[30] T. Hayat, S. Farooq, A. Alsaedi and B. Ahmad, Numerical analysis for radial MHD and mixed convection effects in peristalsis of non-Newtonian nanomaterial with zero mass flux conditions, *Results Phys.,* **7** (2017) 451-458.

[31] T. Hayat, S. Asghar, A. Tanveer and A. Alsaedi, Outcome of slip features on the peristaltic flow of a Prandtl nanofluid with inclined magnetic field and chemical reaction. *Eur. Phys. J. Plus*, **132** (2017) 217.

[32] T. Hayat, H. Zahir, A. Tanveer and A. Alsaedi, Radial magnetic field and convective condition aspects for the peristalsis in a curved channel with compliant properties. *Eur. Phys. J. Plus,* **132** (2017) 12.

[33] N. Ali, Z. Asghar, O. Anwar Bég and M. Sajid, Bacterial gliding fluid dynamics on a layer of non-Newtonian slime: Perturbation and numerical study. *J. Theoretical Biology,* **397** (2016) 22–32.

[34] Z. Asghar, N. Ali, and M. Sajid, Interaction of gliding motion of bacteria with rheological properties of the slime. *Math. Biosci.*, **290** (2017) 31–40.

[35] Z. Asghar, N. Ali, O. Anwar Bég and T. Javed, Rheological effects of micropolar slime on the gliding motility of bacteria with slip boundary condition. *Results Phys.*, **9** (2018) 682–691.

[36] M. Waqas, M. I. Khan, T. Hayat and A. Alsaedi, Numerical simulation for magneto Carreau nanofluid model with thermal radiation: A revised model, *Computer Methods Appl. Mech. Eng.*, **324** (2017) 640-653.

[37] M. Waqas, A. Alsaedi, S. A. Shehzad, T. Hayat and S. Asghar, Mixed convective stagnation point flow of Carreau fluid with variable properties, *J. Braz. Soc. Mech. Sci. Eng.*, **39** (2017) 3005-3017.

[38] S. Sudo, S. Segawa and T. Honda, Magnetic swimming mechanism in a viscous liquid, *J. Intell. Mater Syst. Struct.* **17** (2006) 729–736.

[39] F.Z. Temel and S. Yesilvurt, Confined swimming of bio-inspired magnetic micro-swimmers in rectangular channels, *67th Annual Meeting of the APS (American Physical Society) Division of Fluid Dynamics, San Francisco, California*, *November* (2014).

[40] F.Z. Temel, A.E. Bezer and S. Yesilvurt, Navigation of mini-swimmers in channel networks with magnetic fields, *IEEE (Institute of Electrical and Electronics Engineers), Int Conf Robotics and Automation (ICRA 2013), USA, May* (2013).

[41] D.R. Bond, Electrode-reducing microorganisms that harvest energy from marine sediments, *Science* **295** (2002) 483–485.

[42] D.R. Lovely, The microbe electric: Conversion of organic matter to electricity, *Curr Opin Biotechnol.*, **19** (2008) 564–571.

[43] A.R. Ansari, A.M. Siddiqui and T. Hayat, An analysis of the swimming problem of a singly flagellated micro-organism in an MHD fluid, *Nonlinear Dyn* **51** (2008) 477–481.

[44] A.R. Ansari, A.M. Siddiqui and T. Hayat, An analysis of the swimming problem of a singly flagellated micro-organism in an MHD fluid flowing through a porous medium, *Nonlinear Anal Real World Appl* **11** (2010) 22–28.

[45] H. Gadelha, On the optimal shape of magnetic swimmers, *Regul Chaotic Dyn* **18** (2013) 75–84.

[46] M. Belovs and A. Cebers, Ferromagnetic microswimmer, *Phys Rev E,* **79** (2009) 051503.

[47] W. Gao, D. Kagan, O. S. Pak, C.Clawson, S. Campuzano, E. Chuluun-Erdene, E. Shipton, E. E. Fullerton, L. Zhang, E. Lauga and J. Wang, Cargo-towing fuel-free magnetic nanoswimmers for targeted drug delivery, *Small* **8** (2012) 460–467.

[48] E. Gauger, M. Downton and H. Stark, Fluid transport at low Reynolds number with magnetically actuated artificial cilia, *Eur Phys J. E* **28** (2009) 231–242.

[49] D. Tripathi, R. Jhorar, A. Borode and O. Anwar Bég, Three-layered electro-osmosis modulated blood flow through a microchannel, *European Journal of Mechanics - B/Fluids 72* (2018), 391-402.

[50] G. Loget and A. Kuhn, Propulsion of micro-objects by dynamic bipolar self-regeneration, *J. Amer. Chem. Soc.,* 132 (2010) 15918-15919.

[51] O. Anwar Bég, Multi-physical electro-magnetic propulsion fluid dynamics: mathematical modelling and computation, *Mathematical Modeling: Methods, Applications and Research, W. Willis and Seth Sparks (Editors), Chapter 1, 1-88, Nova Science, New York, USA* (2018).

[52] V K Narla, Dharmendra Tripathi, O. Anwar Bég and A Kadir, Modelling transient magnetohydrodynamic peristaltic pumping of electroconductive viscoelastic fluids through a deformable curved channel, *Journal of Engineering Mathematics*, 111 (2018), 127-143**.**

[53] Z. Asghar, N. Ali, and M. Sajid, Mechanical effects of complex rheological liquid on a microorganism propelling through a rigid cervical canal: swimming at low Reynolds number. *J. Braz. Soc. Mech. Sci. & Eng.*, 40 (2018) 475 (1-16).